Geophys. J. Int. (2005) **160,** 815–832 doi: 10.1111/j.1365-246X.2005.02550.x

The lepidocrocite–maghemite–haematite reaction chain—I. Acquisition of chemical remanent magnetization by maghemite, its magnetic properties and thermal stability

T. S. Gendler, [1] V. P. Shcherbakov,[2] M. J. Dekkers,[3] A. K. Gapeev,[2] S. K. Gribov[2] and E. McClelland[4]

[1] *Institute of Physics of the Earth, Moscow, Russia*
[2] *Geophysical Observatory 'Borok', Borok, Russia*
[3] *Paleomagnetic Laboratory 'Fort Hoofddijk', Department of Earth Sciences, Utrecht University, Utrecht, the Netherlands. E-mail: dekkers@geo.uu.nl*
[4] *Department of Earth Sciences, Oxford University, Oxford, UK*

Accepted 2004 December 8. Received 2004 November 5; in original form 2004 July 8

SUMMARY

We report on the magnetic properties and the acquisition of a chemical remanent magnetization (CRM) in a field of 100 μT as a function of temperature and time during the lepidocrocite–maghemite–haematite reaction chain. The development of CRM was monitored at a series of 13 temperatures ranging from 175 to 550 °C; data acquisition was done at the specific formation temperatures for durations of up to 500 hr. Up to acquisition temperatures of 200 °C it takes a considerable time (up to 7 hr) before the CRM is measurable. This time decreases with increasing temperature, reflecting the activation energy of the reaction to form the first maghemite. During the lepidocrocite conversion, formation of two types of maghemite is suggested by two peaks in the CRM versus time curves.

Magnetic properties were analysed after various stages in the reaction. They indicate a mixture of superparamagnetic and single-domain maghemite. The first reaction product (obtained after annealing at 200 °C) is a fine-grained yet crystalline maghemite (labelled type A). Before massive maghemite formation occurs, the coercive and remanent coercive forces go through a minimum at intermediate temperatures of 250–300 °C (annealing for 2.5 hr). This minimum lowers to 200–250 °C with increasing annealing time (500 hr). This is probably the result of two processes acting simultaneously—formation of superparamagnetic maghemite particles of a second less crystalline maghemite type (labelled type B) and removal of stacking faults in type A maghemite. The second process is suggested by analogy to the behaviour of natural magnetite/maghemite systems on annealing. Removal of stacking faults is reported to result in a magnetic softening of the grain assemblage. Annealing at 300–350 °C removes most of the lepidocrocite and the second maghemite type, type B, becomes prominent. Haematite formation sets in at slightly higher temperatures, yet the type B maghemite is in part thermally stable up to 600 °C enabling Thellier–Thellier experiments. This stability is also inferred from Arrhenius fitting that shows a comparatively high activation energy for the maghemite to haematite reaction. In Thellier–Thellier experiments the CRM showed a markedly downward convex Arai–Nagata plot while a second thermoremanent magnetization (TRM) showed perfect linear behaviour as expected. This feature may be used to recognize CRM in natural rocks.

Key words: chemical remanent magnetization, lepidocrocite, maghemite, red beds, thermal stability.

1 INTRODUCTION

Continental red beds make up a significant proportion of the sedimentary record, particularly in the Palaeozoic and Mesozoic. As a rule they are relatively strongly magnetized. Hence, red beds constitute an important target for palaeomagnetic studies. They are formed in a wide range of tectonic settings in deltaic, alluvial or aeolian environments, and in both arid and moist climates. The reddening induced by pigmentary haematite is now generally considered to be diagenetic in origin. Detrital magnetite and early created ferric oxyhydroxides with maghemite may be transformed into haematite yielding a chemical remanent magnetization (CRM). The natural

remanent magnetization (NRM) of a red bed is thus bound to consist of more than one component. To interpret the geological history of the rock from the various superimposed magnetizations, the acquisition mechanism and age of each NRM component must be determined. With this information, the tectonic and magnetostratigraphic implications can be assessed.

In addition to magnetite of detrital origin, the NRM of red beds is carried predominantly by haematite and maghemite. Diagenetic processes have been shown to be important in the development of the latter two mineral types. In particular, the formation of maghemite and haematite can proceed by dehydroxylation of the iron oxyhydroxides α-FeOOH (goethite) and γ-FeOOH (lepidocrocite). Previous work (e.g. Bagin 1967; Hedley 1968; Sakash & Solntseva 1971; McClelland & Goss 1993; Özdemir & Dunlop 1993; Gehring & Hofmeister 1994; Gendler *et al.* 1999) has shown that the CRM properties of reaction products are dependent on the starting materials and their particle size. Also reaction temperature, atmosphere and annealing time were shown to be important parameters.

Here we report on an investigation of the magnetic mineralogy during the lepidocrocite–maghemite–haematite reaction chain along with the properties of the CRM acquired at different stages during this transformation. Experiments included a thermomagnetic study of the saturation magnetization and initial susceptibility of the minerals formed at different stages during the transformation reactions to follow the appearance, content, properties and decay of the various magnetic phases. A second set of experiments involved the continuous monitoring of CRM acquisition during long runs of up to 500 hr performed at elevated temperatures T_{CRM} ranging from 175 to 550 °C, hence at different stages of the transformation. The aims of these experiments were to determine the kinetic characteristics of the lepidocrocite transformation process as a function of T_{CRM} and to study magnetic properties and thermal stability of the CRMs obtained. Finally, 'Thellier–Thellier palaeointensity experiments' were carried out on the CRM obtained on the maghemite that appeared to be in part remarkably thermally stable. This enabled comparison of CRM and thermoremanent magnetization (TRM) as 'primary' NRM in Arai–Nagata plots.

2 LEPIDOCROCITE AND MAGHEMITE

In lepidocrocite, the double bands of iron–oxygen octahedra share edges to form zigzag layers that are connected to each other by hydrogen bonds (OH–O). The layer structure of lepidocrocite is energetically less stable than the framework structure of goethite. Lepidocrocite is crystallographically analogous to boehmite (γ-AlOOH). Because of the oriented hydroxyl bonds, the layer structure of lepidocrocite (boehmite) is not completely close-packed. Half of the oxygen atoms are located inside the octahedral layers and half are on the surface, and only the latter are associated with hydrogen. Within the layers the oxygen atoms are in cubic close packing. So, the γ-series oxyhydroxides and oxides of Al and Fe (boehmite, lepidocrocite, γ-Al_2O_3 and γ-Fe_2O_3) are based on oxygen ions in cubic close packing (Ewing 1935; Ervin 1952). Lepidocrocite is a common minor constituent in redoxomorphic soils (seasonal change of oxidizing and reducing environment) in both temperate and humid climates (Schwertmann 1988; Cornell & Schwertmann 1996).

Chuhrov *et al.* (1975a,b) summarized various experiments on iron hydroxide synthesis. They showed that lepidocrocite can be easily produced at ambient temperatures from different ferrous compounds oxidizing in hypergenic or supergenic zones. Control of the pH was shown to be essential in the lepidocrocite formation reaction (see also Schwertmann & Cornell 1991). pH should be close to neutral and the oxidation reaction rate should be moderate. This leads to green rust formation, a precursor of lepidocrocite. In nature, lepidocrocite formation is often connected with the hypergenic alteration of siderite and other carbonates; iron is released to fluids as $Fe(HCO_3)_2$. Chuhrov *et al.* (1975a,b) supposed that a characteristic feature of lepidocrocite as a mineral phase would be a deficit of Fe atoms leading to the appearance of vacancies. So, line broadening in X-ray diffractograms is not due to small crystallite size only. Often lepidocrocite also contains extra H_2O and has a distinctly varying crystallinity (De Grave *et al.* 1986).

2.1 Decomposition products

The thermal decomposition of synthetic and natural lepidocrocite has been studied by a substantial number of researchers using different techniques such as electron and X-ray diffraction (XRD) (Takada *et al.* 1964), infrared (IR) and Mössbauer spectroscopy (Sakash & Solntseva 1971; Subrt *et al.* 1981; De Bakker *et al.* 1991; Gehring & Hofmeister 1994), thermogravimetric analysis (TGA) and calorimetry (Giovanoli & Brütsch 1975; Von Keller 1976; Laberty & Navrotsky 1998) and magnetic measurements (Bagin 1967; Sakash & Solntseva 1971; McClelland & Goss 1993; Özdemir & Dunlop 1993; Gehring & Hofmeister 1994; Gendler *et al.* 1999).

The enthalpy of the dehydroxylation reaction of α-FeOOH to $\frac{1}{2}\alpha$-Fe_2O_3 is 13.5 kJ mol^{-1} and that of γ-FeOOH to $\frac{1}{2}\gamma$-Fe_2O_3 is 5.1 kJ mol^{-1} (Laberty & Navrotsky 1998). So, lepidocrocite can be converted to goethite *in situ* if the reaction rate were very slow. The usual phase transition of lepidocrocite, however, is the dehydroxylation reaction as in goethite. For γ-FeOOH, in contrast to α-FeOOH, this transformation occurs in three steps. The first step is attributed to desorption of physisorbed (weakly bound) molecular water, the second step corresponds to the dehydroxylation of iron oxyhydroxide to γ-Fe_2O_3 and the third step is the transition of γ-Fe_2O_3 to α-Fe_2O_3.

The transition from the hydrated to the dehydrated phase is topotactic, i.e. the oxygen framework remains intact while the hydroxyl groups are removed and the iron atoms are redistributed. Dehydroxylation requires the removal of one-quarter of the oxygen atoms. As was suggested by Ervin (1952), half of the surface oxygen atoms would be lost while oxygens from the interior of the layers would remain unaffected. It is conceivable that after this oxygen removal, the layers would amalgamate to a completely cubic close-packed oxygen network. In the case of lepidocrocite, the distribution of the Fe atoms would be random and atoms would have to migrate through the oxygen framework to reach stable positions. This mechanism implies that lepidocrocite is not decomposed simply to γ-Fe_2O_3, but that a series of distinct dehydrated phases can be produced. All of them will have oxygen in cubic close-packed positions and Fe cations in the interstices of the network. The difference will be only in the arrangement of the metallic ions and in their degree of ordering. For heated boehmite, these variably disordered and ordered modifications were detected by XRD experiments which showed reflections deriving from a more complex symmetry than that of the classic spinel structure (Ervin 1952).

Maghemite formed by the calcination of lepidocrocite at comparatively low temperatures, however, is reported to have a structure with ordered vacancies because the cation configuration of the parent material is preserved (Takei & Chiba 1966). At higher temperature this ordered structure can be transformed into a disordered one. In contrast, Bernal *et al.* (1957) reported that disordered γ-Fe_2O_3 was obtained by careful calcination of γ-FeOOH at 250 °C. The

problem of the vacancy distribution in maghemite has been discussed for many years (e.g. Annersten & Hafner 1973; Waychunas 1991). The vacancy distribution is strongly related to the method of preparation of the maghemite and its parent material. Different sets of superstructure lines were reported, either consistent with a cubic primitive lattice (five possible space groups) or a tetragonal lattice (Van Oosterhout & Rooijmans 1958; Annersten & Hafner 1973). Brown (1952) suggested the space group $P4_132$ for his maghemite sample, which contained some structural H_2O. This suggestion is important for the maghemite formed from heating lepidocrocite at moderate temperatures. Maghemites formed along this pathway can thus show a variable degree of vacancy ordering.

In four well-defined synthetic lepidocrocite samples, the onset of the weight loss indicative of incipient maghemite formation was observed at about 200 °C (De Bakker *et al.* 1991). The electron paramagnetic resonance (EPR) spectrum of synthetic lepidocrocite was found to start changing after heating at 175 °C while IR spectra (sensitive to small changes in the content and distribution of structural water and hydroxyl groups) already demonstrated substantial variations in a temperature range from 155 to 176 °C (Gehring & Hofmeister 1994). The temperature at which maximum weight loss occurs in TGA curves (T_{TGA}) varied from 211 to 250 °C for different synthetic lepidocrocite samples and from 280 to 306 °C for various crushed natural samples (Von Keller 1976; De Bakker *et al.* 1991). Sakash & Solntseva (1971), however, determined that T_{TGA} changes from 230 to 280 °C when the heating rate is increased from 10 to 66 °C min^{-1}. Hence, the starting temperature of the dehydroxylation reaction and its further development depend strongly on the initial lepidocrocite, sample preparation, heating rate and heating procedure (stepwise or continuous), etc. The activation energy of the lepidocrocite dehydroxylation reaction varies from 13.1 to 26.7 kcal mol^{-1} depending on the crystallinity of the lepidocrocite (Von Keller 1976).

Sakash & Solntseva (1971) did not observe any structural change in synthetic lepidocrocite annealed at 105 °C for 227 hr. During the course of the lepidocrocite dehydroxylation maghemite starts to appear in the interval ranging from 200 to 300 °C. Its formation process is not straightforward though, with a pathway going through various intermediate stages. On the molecular level, it was shown that removal of OH groups in lepidocrocite begins at 142–155 °C (Gehring & Hofmeister 1994). In that temperature range they observed the decrease of three IR peaks (at 739, 1015 and 1159 cm^{-1}) assigned to δ-OH bending bands (Lewis & Farmer 1986). The decrease was more pronounced after heating at 176 °C. Gehring *et al.* (1990) argued for the creation of an activated stage at this temperature. In these studies lattice changes were not discerned below 199 °C. Hence, the loss of water also occurs prior to the formation of maghemite, which indicates the actual dehydroxylation of the lepidocrocite structure.

The difference between the temperatures at which OH groups start to be removed from the structure and the formation of maghemite is most likely related to the time needed for OH^- and H^+ to combine to form H_2O, and its subsequent diffusion (Gehring & Hofmeister 1994). A so-called activated intermediate state is created by the dehydroxylation process that precedes the structural transformation of lepidocrocite to maghemite (Gehring *et al.* 1990). IR spectra show first an increase of the Fe–O distance followed by a decrease and the generation of an imperfect maghemite structure tied to superparamagnetic (SP) maghemite clusters (Gehring & Hofmeister 1994). During this stage the specific surface area increases from 27 to 47.5 $m^2\ g^{-1}$ and even to 60.7 $m^2\ g^{-1}$ (Sakash & Solntseva 1971; Laberty & Navrotsky 1998).

2.1.1 Maghemite crystallite size and microstructure

The size of maghemite particles produced from lepidocrocite is usually <10 nm; it is independent of the grain size of the initial lepidocrocite (De Bakker *et al.* 1991). Also Bernal *et al.* (1957) obtained small maghemite crystallites of about 5 nm in size. Takada *et al.* (1964) concluded from X-ray and electron diffraction experiments on maghemite crystallites (obtained from plate-like lepidocrocite) that small γ-Fe_2O_3 crystallites with an average diameter of about 6 nm link together to form highly oriented aggregates whose shape resembles the morphology of the original lepidocrocite crystallites. This mechanism causes a strong magnetic interaction between the particles. Under transmission electron microscopy (TEM) the maghemite particles appear as agglomerates of a large number of very small, needle-shaped crystallites (Lepin' & Ruplis 1971; McClelland & Goss 1993). These authors observed that upon annealing a porous angular microstructure formed perpendicular to (002) lepidocrocite planes. The size of the pores increases with annealing from 1.7–4 nm (180–350 °C) to 6–7 nm (400 °C) along with an increase in size of the maghemite nanoparticles from ∼4 to ∼6 nm. The major influence of porosity and defects on the magnetic properties of maghemite and the stability of its magnetic record were pointed out by Morales *et al.* (1998).

Maghemite is thermodynamically metastable with respect to haematite, yet it can possess a remarkable thermal stability. Widely varying γ to α transition temperatures (labelled GAT temperature by De Bakker *et al.* 1991) have been reported ranging from room temperature to 900 °C. A number of factors like the method of preparation, grain size and shape, impurities, reaction pressure, reaction atmosphere and annealing time, have been put forward as an explanation for this wide range. For example, Imaoka (1968) found at atmospheric pressure a GAT of 560 °C for acicular γ-Fe_2O_3 particles but 250 °C for granular particles. Takei & Chiba (1966) suggested this temperature interval to range from 250 to 600 °C. Özdemir & Banerjee (1984) reported on a maghemite that was thermally more or less stable to heating in air up to 600–640 °C; complete transformation to haematite required temperatures higher than 660 °C. The presence of Al in the structure stabilizes maghemite (e.g. De Boer & Dekkers 1996).

Pressures of 150 MPa caused a lowering of the inversion temperature to 0 °C (Kushiro 1960). In a series of experiments with changing annealing time or pressure, Adnan & O'Reilly (1999) monitored GAT using magnetic properties as a proxy for the γ-Fe_2O_3 concentration during the inversion process (acicular maghemite with an aspect ratio of 6:1). The GAT process appears to be thermally activated, and Adnan & O'Reilly (1999) experimentally calculated an activation energy of 3.7 eV at atmospheric pressure and of 0.5 eV at a pressure of about 150 MPa. They pointed out that the presence of defects strongly affects the activation energy, which results in variation of the inversion behaviour of nominally similar materials.

Van Oorschot & Dekkers (1999) showed that the stability of maghemite (formed from magnetite by oxidation in air) varied substantially as a function of the heating atmosphere. In argon maghemite was reasonably stable against heating cycles up to 700 °C, while in air complete transformation was already obtained above 550 °C.

Adnan & O'Reilly (1999) suggested that the amount and types of internal defects in the maghemite would be crucially dependent on its preparation method. The role of the defects would be more important than that of grain size or surface area of the particles. Therefore, we will concentrate here on the GAT temperature observed for maghemite obtained by calcination of lepidocrocite. This

temperature is also reported to vary depending on starting material, maghemite concentration, reaction atmosphere, heating procedure (gradually increasing, stepwise increasing or just annealing at one specific temperature) and measurement method. For instance, Bagin (1967) reported a GAT temperature interval for bulk natural lepidocrocite heated stepwise in air of 375–575 °C based on XRD and isothermal remanent magnetization (IRM) measurements. The same lepidocrocite sample heated stepwise in vacuum did not show an IRM decrease until annealing at 600 °C (Rybak 1971). Using IR spectra and IRM measurements, Sakash & Solntseva (1971) observed the GAT for synthetic lepidocrocite (10 nm) in a narrow temperature interval of 315–350 °C in a stepwise annealing experiment. For the same samples, TGA measurements indicated the maximum rate of the GAT to occur at 237 °C for a heating rate of 4.5 °C min^{-1} and at 350 °C for a heating rate of 10 °C min^{-1}. Higher GAT temperatures varying from 435 to 485 °C were found by De Bakker *et al.* (1991), who also used TGA (heating rate ∼2 °C min^{-1}) to monitor the behaviour of four synthetic lepidocrocite samples. The GAT temperature correlated with the excess H_2O in the original lepidocrocite: the smaller the amount the higher the GAT temperature. The incorporation of more OH^- ions causes an increase of the number of defects in the maghemite lattice which favours a lowering of the GAT temperature by accelerating the transformation process.

In the same sample set De Bakker *et al.* (1991) varied the annealing rates. For rates >2°C min^{-1} they determined the simultaneous presence of maghemite and haematite by XRD and Mössbauer spectroscopy after annealing at 337–420 °C. Gehring & Hofmeister (1994) studied the behaviour of synthetic lepidocrocite samples after stepwise heating between 100 and 500 °C (0.5 hr at each temperature). They observed a complete structural conversion of maghemite to haematite at 500 °C using EPR spectra and at 600 °C according to bulk susceptibility measurements. During thermomagnetic measurements (steadily increasing temperature) this lepidocrocite showed a GAT ranging from 273 to 450 °C.

McClelland & Goss (1993) also observed a variation of the GAT temperature interval for tightly packed and dispersed (3.86 per cent by weight) synthetic lepidocrocite: 370–450 °C and 442–591 °C respectively. Hence, the temperature cannot be used as an absolute measure of the transformation progress, which appears to be slower in dispersed samples than in pure samples. The same observation was made by Özdemir & Dunlop (1993) who obtained a GAT interval ranging from 480 to 560 °C for undispersed lepidocrocite and from 550 to >653°C for samples containing 2 per cent by weight. Hence, the simultaneous presence of both α- and γ-Fe_2O_3 can occur over a significant temperature interval. Bagin (1967) and McClelland & Goss (1993) concluded on the basis of magnetic measurements only that inversion to haematite might begin before all lepidocrocite has transformed to maghemite. This assumption was not confirmed by direct methods such as XRD, IR or Mössbauer spectroscopy. One of the aims of this study was to check the possibility and conditions of a simultaneous presence of all three phases—lepidocrocite, maghemite and haematite.

Magnetic determination of maghemite relies in part on the determination of its Curie temperature (T_C). It is rather difficult to determine experimentally because of the transformation to haematite. A formal Curie temperature can be only measured on a thermally stable maghemite. Various Curie temperatures from 400 to 645 °C have been reported for maghemites of different origin. Maghemite produced by oxidation of magnetite in air was reported to be mainly cubic without clear superstructure with T_C close to 640–645 °C (Heider & Dunlop 1987; Özdemir & Banerjee 1984; Van Oorschot & Dekkers 1999). Maghemite obtained by oxidation of synthetic cubic magnetite grown in aqueous solution had a T_C of 602–614 °C (Özdemir & Dunlop 1989). A T_C of 575 °C was observed by Aharoni *et al.* (1962) for maghemite obtained by annealing α-Fe_2O_3 in H_2. Minor Sn impurities in the maghemite (γ-$Fe_{1.9}Sn_{0.1}O_3$) lowered T_C to an interval between 477 and 547 °C for synthetic particles of 44–46 nm (Berry & Helgason 2000). Single-crystal films grown by different methods on MgO single crystals showed also a low T_C in an interval of 405–470 °C. These low T_C values were observed for thin films with a disordered cubic crystal structure (Takei & Chiba 1966) and with an ordered tetragonal lattice (Barinov 1982; Babkin *et al.* 1991).

2.1.2 Haematite

The haematite grains forming from lepidocrocite via maghemite are well-crystallized with sizes distinctly larger than that of the preceding maghemite particles. Feitknecht & Mannweiler (1967) proposed that 50–100 neighbouring maghemite crystallites of about 5 nm would finally transform into one large haematite particle. As a rule, X-ray diffraction shows fairly sharp haematite reflections, also just after the appearance of haematite. They become sharper at the final stage of the transformation reactions. McClelland & Goss (1993) observed by TEM the formation of haematite single crystals from polycrystalline aggregates of maghemite. These single crystals had the same shape and size as their acicular lepidocrocite precursor (2000 × 70 nm). They estimated the blocking temperature (T_b) of acicular haematite with dimensions 0.07 × 1.5 μm to be 640–650 °C. Such reduced values of T_b are very often observed in red sandstones. Özdemir & Dunlop (1993) suggested that the blocking temperature of haematite crystallites appearing in high-temperature runs (>450 °C) is about 625 °C. The size of their initial lepidocrocite particles was 30 nm × 400–900 nm. However, it is not common that haematite formed from lepidocrocite has the same grain size as the initial lepidocrocite.

The particle sizes are often estimated from X-ray diffraction. De Bakker *et al.* (1991) observed haematite with a mean crystallite diameter (MCD) of 8–35 nm after the 337–380 °C runs and haematite with a MCD of 35–72 nm at the final stage of reaction. The average particle diameters estimated from TEM data was in good agreement with the X-ray data. The haematite particles in their experiments were almost spherically shaped and did not exhibit any macropores. In spite of their rather big particle size and high crystallinity, the haematites showed a 15–45 °C decrease of their Morin transition temperature. This was explained by relative lattice dilatation.

Thus the main feature of the haematite formed from lepidocrocite via maghemite is its higher degree of crystallinity and its larger particle size compared with its parent maghemite. The considerable difference in crystallite sizes between maghemite and haematite in this reaction is tied to the chain mechanism of interaction of small maghemite particles (Takada *et al.* 1964; Berkowitz *et al.* 1968; Morrish & Clark 1974). This mechanism allows small nominally SP maghemite grains to act as one bigger magnetic particle to acquire a CRM (McClelland & Goss 1993).

2.2 CRM formation in the iron oxyhydroxide dehydroxylation reaction chain

In the first, to our knowledge, study of CRM (Bagin 1967) acquired during the transition of goethite to haematite and of lepidocrocite via maghemite to haematite, a significant difference in the properties of these CRMs was revealed. The characteristics of the CRMs could not be described unambiguously by a simple grain-growth mechanism (*cf.* Haigh 1958; Kobayashi 1961; Stokking & Tauxe 1987).

Grain-growth CRM is largely equivalent to a TRM and the parent phase has no influence on the properties of the CRM of the daughter phase. If the parent material is magnetic, more complex situations result and the direction and properties of the CRM may be influenced by the parent material, for instance when maghemite is forming from magnetite by oxidation (e.g. Heider & Dunlop 1987). This situation is referred to as alteration CRM by Stokking & Tauxe (1987) and sometimes as crystallization remanent magnetization (Dunlop & Özdemir 1997).

The CRM behaviour during lepidocrocite decomposition was also studied by Hedley (1968) and more recently in detail by Özdemir & Dunlop (1993) and McClelland & Goss (1993). Hedley (1968) observed very different magnetic behaviour on two series of synthetic lepidocrocite samples with different grain size and shape. 'Cornflake'-like particles with crystallite sizes of about 10 nm showed clearly the production of SP maghemite of the same size as the initial material. A maximum remanence σ_r of about 10^{-3} A m^2 kg^{-1} was obtained, and no self-reversal occurred during the GAT. Acicular particles of lepidocrocite (250 × 15 nm) exhibited a much higher σ_r (∼0.3 A m^2 kg^{-1}) and a remanence self-reversal for T_{CRM} between 522 and 630 °C. Hedley (1968) suggested that exchange interaction would be more plausible than magnetostatic interaction as a cause for the self-reversal. The experimental results of Özdemir & Dunlop (1993) and McClelland & Goss (1993) agree by and large. However, some intriguing differences should be noted. McClelland & Goss (1993) observed a wide temperature interval of the CRM formation (T_{CRM} of 250–550 °C) in which the obtained CRM intensity was high. For T_{CRM} between 572 and 591 °C, even a complete self-reversal of the CRM was documented similar to the results of Hedley (1968). They attributed the self-reversal to negative exchange coupling between the parent maghemite and daughter haematite phases. Özdemir & Dunlop (1993) found a two-peak pattern in values of CRM intensity upon T_{CRM} with a prominent intervening minimum. As an explanation they suggested the presence of negative exchange coupling between regions of maghemite separated by antiphase boundaries. They observed that the CRM produced in runs up to 450 °C was univectorial with the remanence parallel to the applied field. It became bivectorial between the 500 and 653 °C runs and neither CRM vector was parallel to the applied field. After the 555 °C run an internal self-reversal was observed. They also suggested the existence of exchange coupling between the maghemite and haematite lattices. As explanation of the partial or full self-reversal Özdemir & Dunlop (1993) argue that at T_{CRM} blocked and unblocked maghemite regions would coexist with haematite crystallites that are below their blocking temperature. Thus, these authors concluded that the common working assumption of a simple grain-growth CRM mechanism should be reconsidered in the case of the γ-FeOOH transformation process.

3 SAMPLES AND EXPERIMENTAL PROCEDURES

For the experiments we used three synthetic lepidocrocite samples labelled L1, L2 and L3, and one natural lepidocrocite sample labelled Ln. The synthetic samples were prepared from a solution of iron (II) sulphate mixed with solutions of potassium iodate and sodium thiosulphate at 45 °C as described by De Grave *et al.* (1986). Three different batches with varying ferrous sulphate concentration were prepared. The crystallinity and particle size of the initial samples were analysed using XRD. X-ray diffractograms of two initial synthetic lepidocrocites (L1 and L2) were recorded at the Geophysical Observatory Borok using a DRON-2 diffractometer with Co K_α radiation, with a scan speed of 1° min^{-1} for 2θ angles from 13 to 82°; NaCl was used as the internal standard. X-ray patterns of the third synthetic sample (L3) and the natural sample were measured using a Philips PW1700 diffractometer and Cu K_α radiation at the Department of Earth Sciences, Utrecht University (stepscan 0.02° 2θ, 1 s counting time per step; no internal standard was added).

Table 1. Crystallinity and crystallite size of the synthetic and natural lepidocrocites.

Sample	*Kr*	*D*
L1	1	70
L2	0.25–0.5	4–6
L3	0.8	35
Ln	0.95	53

Kr, crystallinity according to eq. (1); *D*, average crystallite size in nm. See text for further explanation.

Because different diffractometers were used one cannot directly compare the intensity of corresponding reflections. The crystallinity *Kr* was determined according to eq. (1) as the ratio of the width of lepidocrocite X-ray peaks and the instrumental line width as determined from a highly crystalline material that is assumed to be truly crystalline. $W_{1/2}$ is the width at half peak height.

$$Kr = \frac{W_{1/2\ \text{instrument}}}{W_{1/2\ \text{lepidocrocite}}}. \quad (1)$$

The average crystallite sizes *D* (Table 1) were determined from XRD line broadening of the (200) and (002) reflections using Scherrer's formula (Araki 1989). They vary between 4–6 and 70 nm (Table 1).

L1 appears to be pure; there is no trace of an additional phase in the X-ray diffractogram. The L2 lepidocrocite is poorly crystalline with a smaller number of reflections. Its line broadening is significant (Table 1) and varies with reflection. All reflections with (0*k*0) indices are decreased in intensity or even absent. L3 shows fairly sharp lepidocrocite lines. XRDs of L2 and L3 show some low-intensity goethite reflections as well. Goethite is a rather common by-product of the lepidocrocite synthesis (e.g. Hedley 1968; Schwertmann & Cornell 1991). The Ln sample exhibits sharp lepidocrocite lines only, hence it is pure.

The synthetic lepidocrocite samples L1, L2 and L3 were used for thermomagnetic measurements only. Low-field mass susceptibility was measured as a function of temperature between 20 and 700 °C on an AGICO KLY-3 susceptibility bridge (frequency $\omega = 875$ Hz with a rms peak field of 0.375 mT). A certain amount of the Ln sample was uniformly dispersed in a kaolin matrix for continuous measurements of magnetic susceptibility using a CS2 attachment to a KLY2 susceptibility bridge in the Earth Sciences Department of Oxford University. The contribution of kaolinite to the signal was always less than 0.05 per cent as test runs with pure kaolin showed. Temperature dependence of the saturation magnetization M_s of non-dispersed tightly packed powdered samples of L1 and L2 was measured from 20 to 700 °C using a vibrating sample magnetometer (VSM) in an external magnetic field $H = 0.45$ T (palaeomagnetic laboratory of the Institute of Physics of the Earth (UIPE), Moscow). The same experiments on dispersed L3 and Ln samples were performed with Curie balance devices (at Observatory 'Borok', Russia, the palaeomagnetic laboratory of UIPE, and with the adapted horizontal translation balance at the Fort Hoofddijk palaeomagnetic laboratory, Utrecht University; all balances use $H = 0.3$ T, that in Utrecht cycles between a minimum and maximum field value, 150 and 300 mT respectively).

The natural lepidocrocite Ln is most suited for the CRM experiments because it is well crystallized and has sufficiently large crystallite sizes. Excess water was carefully baked out from dispersed samples before beginning the experiments. Two sets of CRM acquisition experiments (2.5 and 500 hr runs) were accomplished at a series of temperatures (T_{CRM}) ranging from 175 to 550 °C in a 100 μT steady field (H_{CRM}). The samples were made by uniformly dispersing the lepidocrocite particles in a kaolin matrix (1 per cent lepidocrocite by mass) and moulding the mixture into 10 mm cubes. We will refer to them as Lnd samples. The CRM acquisition was monitored during the heating runs, which lasted up to 500 hr. It was monitored at the annealing temperature in closely spaced time intervals. To impart the CRM we used a high-temperature spinner magnetometer specially designed in the Borok Observatory. Its fluxgate sensor surrounds the water-cooling jacket. The noise threshold of the magnetometer is 10^{-3} A m^{-1}, the temperature stability is ± 1 °C for periods of up to weeks. Note that our experiments report for the first time CRM intensities monitored at the acquisition temperature. After cooling each sample in zero field to room temperature (T_r), the CRM was measured again. Following the remanence experiments, room-temperature hysteresis parameters and hysteresis loops were measured for all samples using a VSM with a maximum field of 1.6 T. The M_s and H_c values were calculated from the hysteresis loops after subtraction of the paramagnetic signal.

For the Thellier–Thellier experiments, an induction coil magnetometer designed at the Borok Observatory was used to induce and demagnetize various partial thermoremanent magnetizations (pTRMs). With this PC-controlled instrument, the remanent magnetization of a sample can be monitored and recorded continuously after having switched off the magnetic field during cooling and/or heating. The noise threshold of the magnetometer is 3×10^{-9} A m^2 for a cubic specimen with 1 cm edges. The maximum available external field is 0.2 mT, while the residual field, after the coil is switched off, is less than 100 nT. Related Mössbauer measurements and more extensive XRD data will be detailed in a future contribution.

4 EXPERIMENTAL RESULTS

4.1 Magnetic measurements

The strong-field thermomagnetic curves $M_s(T)$ on heating the samples L1, L2 and Lnd at different rates are shown in Fig. 1. From

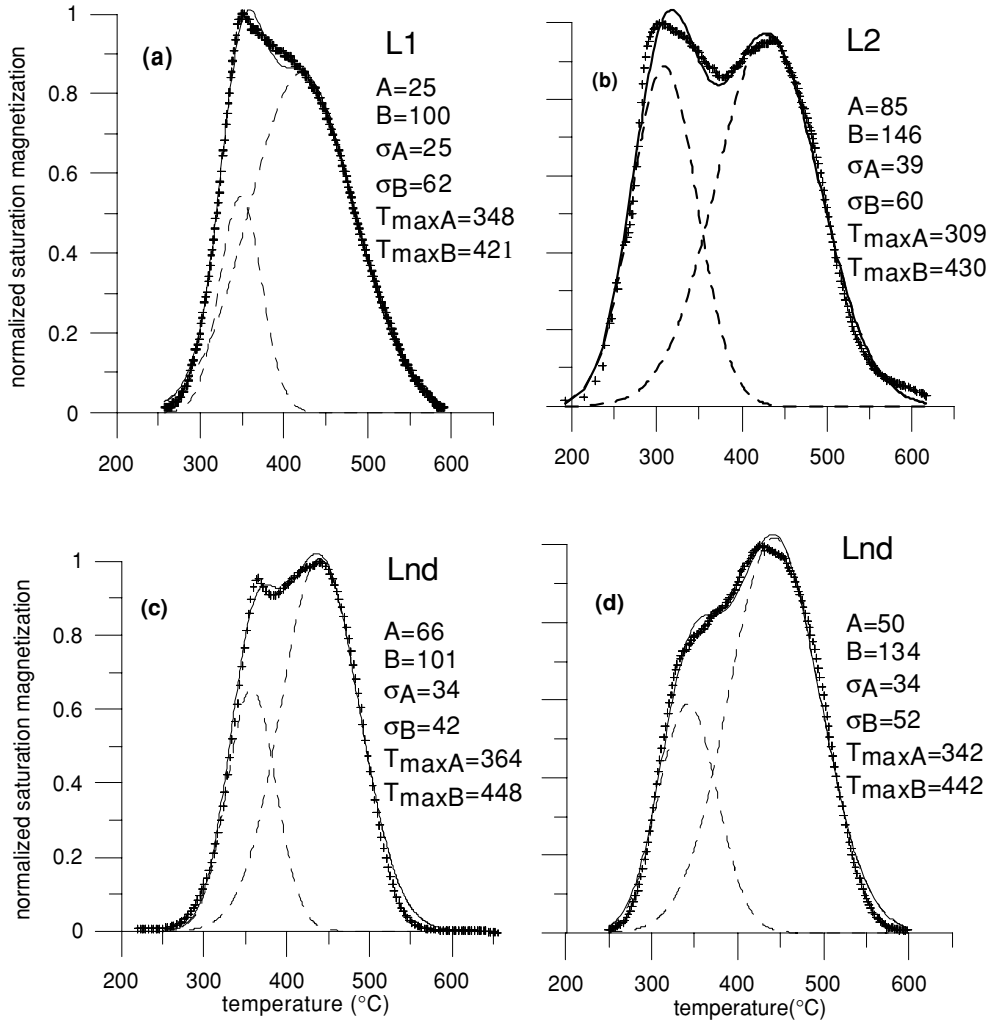

Figure 1. Thermomagnetic curves (plus symbols) acquired in a field of 0.45 T (L1 and L2 lepidocrocite, VSM at UIPE Moscow) or in a field of 0.30 T (Lnd lepidocrocite, Curie balance at Borok). The heating rate (in air) is 0.5 °C s^{-1} for L1 and L2 (a and b); for Lnd it is 1 °C s^{-1} (c) and 5 °C s^{-1} (d). The decomposition of the thermomagnetic curves into Gaussian curves (dashed lines) and the sum of the Gaussians (full lines) is also shown in each panel. The decomposition parameters (according to eq. 2, see text) are shown on the right-hand side of each set of curves.

an initially very low magnetization value, all curves begin to rise steeply at approximately 250 °C, reflecting the start of the conversion of lepidocrocite to maghemite. Note that the poorly crystalline L2 sample starts to rise at 200 °C (Fig. 1b) already testifying to its higher reactivity. Between 350 and 430 °C relatively minor changes in the $M_s(T)$ values occur followed by a quicker decay between 430 and 480 °C. The magnetization decay is probably due to the formation of haematite at the expense of unstable maghemite and/or the approach of the Curie temperature T_C of maghemite which can be as low as ∼420–470 °C when vacancies are confined to one sublattice (Takei & Chiba 1966; Barinov 1982).

The obvious asymmetry of the curves and the occasional appearance of double-peaked $M_s(T)$ curves (Figs 1b and c) suggests the existence of two subsequent stages in the transformation of lepidocrocite to maghemite. For convenience they are labelled A and B stages, with the A stage (or phase) indicating the lowest temperature phase. To describe them formally, we have decomposed the $M_s(T)$ curves into two Gaussian curves (eq. 2): the parameters A, B, σ_A, σ_B, $T_{\max A}$, $T_{\max B}$ of the Gaussians computed for the samples are also shown in Fig. 1

$$M_s(T) = \frac{A}{\sqrt{2\pi}\sigma_A} \exp\left(-\frac{(T - T_{\max A})^2}{2(\sigma_A)^2}\right) + \frac{B}{\sqrt{2\pi}\sigma_B} \exp\left(-\frac{(T - T_{\max B})^2}{2(\sigma_B)^2}\right). \quad (2)$$

The decomposition fits the experimental curves reasonably well. The low-temperature Gaussian might reflect the generation and decay of unstable fine maghemite grains (A phase). The high-temperature Gaussian would then reflect the transformation of the A phase and residual lepidocrocite into a more stable maghemite B phase followed by the conversion to haematite. Independent of the initial lepidocrocite crystallinity, the A stage is always less prominent than the B stage; also the temperature interval in which it exists ($2\sigma_A$), is narrower than that of the B stage. The starting temperature (T_{st}) of the lepidocrocite to maghemite transformation, the width of the characteristic temperature intervals $2\sigma_A$ and $2\sigma_B$, and their mutual relations depend on the samples and heating rate. Indeed, when comparing Figs 1(a) and (b), it becomes apparent that the poorly crystalline lepidocrocite L2 has a lower T_{st} and B/A ratio than the well crystallized L1 sample. Interestingly, the shape of the $M_s(T)$ curves for the Lnd sample varies with heating rate: the low-temperature peak observed at a comparatively low heating rate transforms into a kind of shoulder when the heating rate is higher (*cf.* Figs 1c and d). The relative area of the B phase is expanded by about 40 per cent at the expense of the A phase showing that with higher heating rates the presence of the low-temperature phase can be subdued or even suppressed completely.

The low-field susceptibility versus temperature curves $k(T)$ (see the example of the Lnd sample in Fig. 2a) are more symmetric than the $M_s(T)$ curves. Note the much quicker decay above

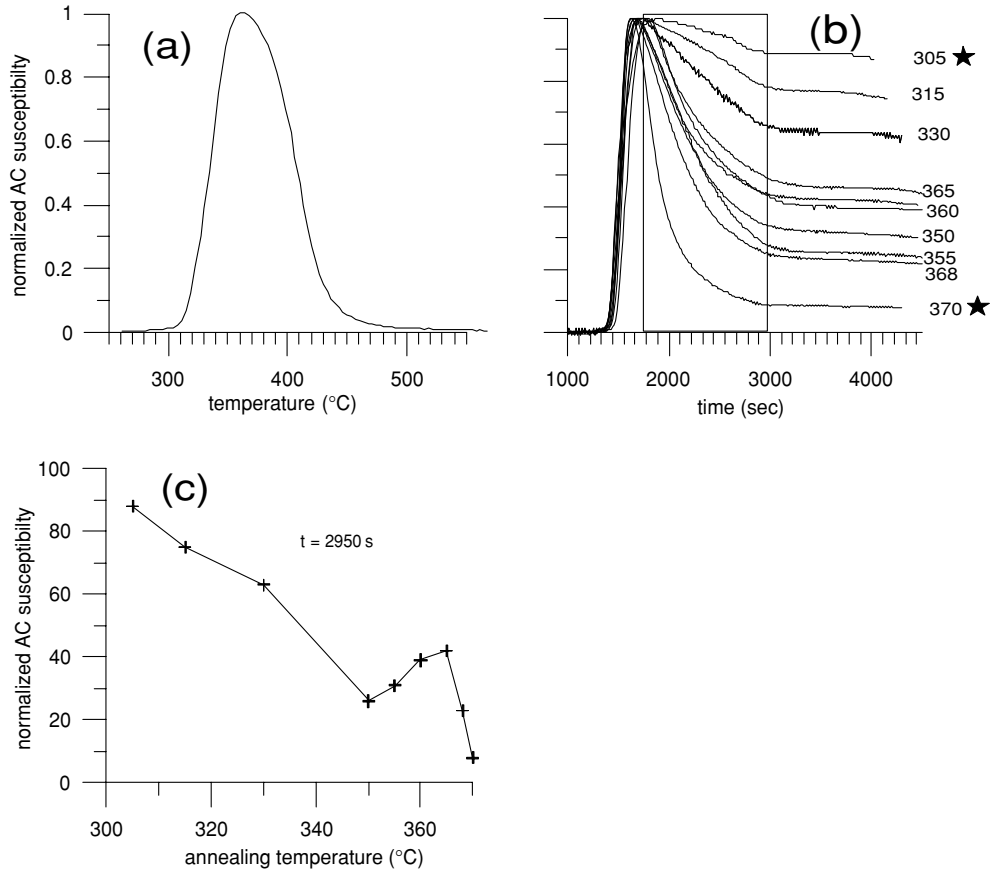

Figure 2. (a) Normalized low-field (alternating current, AC) susceptibility versus temperature for the Lnd sample. The heating rate is 0.3 °C s^{-1}. (b) Annealing behaviour versus time as a function of temperature. Each curve was warmed up to the temperature indicated on its right-hand side (from 0 to 1750 s) after which the temperature was held for about 20 min (from 1750 to 2950 s) and the susceptibility was monitored as a function of time; normalized values are shown. After 2950 s the samples were cooled down. The stars mark the samples taken for Mössbauer experiments (detailed in a future contribution). (c) Normalized AC susceptibility versus temperature after 2950 s showing the differences in conversion rates. At 350 °C reaction progresses more rapidly than at 365 °C, testifying to two maghemite types.

400 °C than that of $M_s(T)$ in Figs 1(c) and (d). To further study the kinetics of the transformations, the low-field susceptibility versus time was monitored during heating, followed by annealing for 20 min at a specified temperature, and cooling down to T_r (Fig. 2b). All $k(t)$ curves show a sharp increase in susceptibility when the temperature reaches ∼300 °C ($t \approx 1400$ s) followed by a decrease in k. The increase indicates the growth of maghemite grains up to the SP threshold size and the decrease in the transformation of maghemite to haematite. The latter is supported by the quick decay of the $k(T)$ curve above 400 °C (Fig. 2a). An interesting feature of the curves in Fig. 2(b) is that the decay rate changes with the annealing temperature. Indeed, the rate first increases with annealing from 300 to 350 °C, then it falls, reaching a minimum at 365 °C. At higher temperatures the decay rate increases again. Fig. 2(c) displays the normalized susceptibility values of Fig. 2(b) after 2950 s (the end of the annealing) versus temperature. The maximum susceptibility at 365 °C, indicating a minimum transformation rate, is evident.

4.2 Magnetic properties of products produced during the lepidocrocite to maghemite transformation

The temperature at which the maghemite is completely transformed to haematite may be quite variable. Nonetheless, after heating at 600 °C during thermomagnetic analysis of tightly packed lepidocrocite only haematite is often observed (McClelland & Goss 1993; Özdemir & Dunlop 1993; Gehring & Hofmeister 1994). The Ln sample behaves in accordance with this common observation but the other samples show a detectable amount of maghemite, even after being heated to 600 °C.

Of course, the majority of unstable A maghemite transforms to haematite during the initial stages of the heating process. Nevertheless, after the first heating in air to 600 °C of L3 lepidocrocite dispersed in kaolin a considerable amount of maghemite remains present judging from the value of $M_s(T_r)$ after cooling the sample (Fig. 3). The sample is stable to reheating: the first cooling and second heating curves are reversible up to 600 °C. Only further heating to 700 °C accomplishes complete conversion of maghemite to haematite. Other examples are shown in Figs 4(a) and (b). In these experiments tightly packed powder of synthetic lepidocrocite samples L1 and L2 was pre-heated to 700 and 600 °C, respectively, before performing the thermomagnetic treatment at a heating rate of ∼0.2 °C s^{-1}. All $M_s(T)$ curves in Figs 3 and 4 demonstrate the presence of a phase with T_C∼ 550 °C, i.e. some part of the maghemite B phase survives heating up to 600 °C. One can argue that the T_C of ∼550 °C would point to magnetite. The appearance of magnetite during the dehydroxylation of lepidocrocite has been reported twice up to now based on Mössbauer spectroscopy data. Rybak (1971) showed that magnetite appeared only upon annealing of lepidocrocite in a vacuum. The appearance of magnetite was also reported by Ona-Nguema *et al.* (2002) during bacterial reduction of lepidocrocite but only when the reduction rate was high. The experimental conditions in those investigations, however, were vastly different from those here. Heating in air makes reduction of ferric iron to ferrous iron highly unlikely.

The content of the maghemite generated after the pre-treatment during the first thermomagnetic run can be roughly estimated from the ratio of the saturation magnetization after the first heating and the peak value of M_s of during the first heating. These ratios are 0.22 for L1 and 0.26 for L2 which both consist of tightly packed lepidocrocite only. So, a noticeable fraction of the maghemite that appeared during the course of the lepidocrocite dehydroxylation survived the heating.

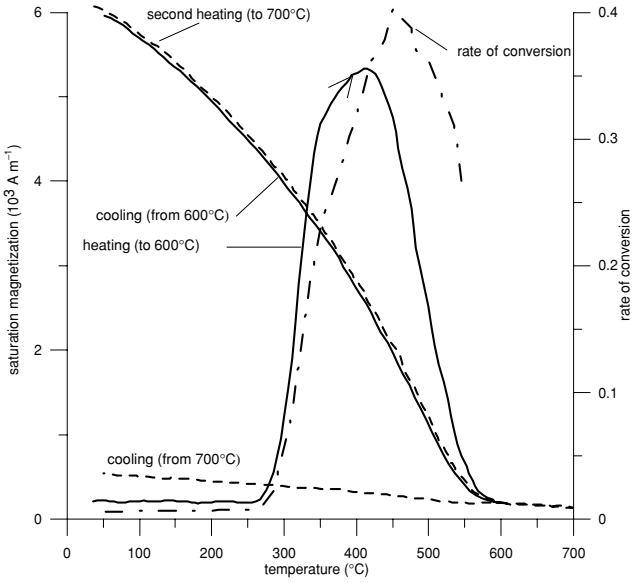

Figure 3. Strong-field thermomagnetic curves of dispersed synthetic lepidocrocite L3 (Curie balance, Borok). Full lines: heating to 600 °C and cooling to T_r. Note that maghemite partially survives heating to this temperature. The long-dash-dotted line indicate the relative content of maghemite created during first heating as calculated in Section 4.1. The short-dashed lines correspond to a second heating to 700 °C and subsequent cooling to T_r. Maghemite does not survive.

This remarkable thermal stability of the maghemite upon heating undoubtedly influences its CRM properties. The thermal stability of the maghemite depends on the lepidocrocite concentration in the starting samples. Also, the maximum temperature of the first heating (the thermal stability during a second heating is of importance for the analysis of CRM properties) is a meaningful factor. Annealing diluted samples at 700 °C for 20 min leads to a complete lepidocrocite via maghemite to haematite reaction. Repeated heating to 600 or 700 °C and cooling of non-diluted lepidocrocite samples preserves part of the maghemite in a thermally very stable state. In earlier studies (Hedley 1968; McClelland & Goss 1993; Özdemir & Dunlop 1993) thermomagnetic analysis was performed on non-diluted samples, hence containing 100 per cent lepidocrocite. CRM acquisition experiments were done with samples containing 50 per cent lepidocrocite (Hedley 1968), 4–8 per cent (McClelland & Goss 1993) and 2 per cent (Özdemir & Dunlop 1993).

4.3 CRM experiments

For the first set of experiments, the CRM acquisition versus time was monitored at frequent intervals directly at the acquisition temperature for 500 hr (except for the 235 °C run which lasted for only 2.5 hr for technical reasons). The corresponding curves are shown in Fig. 5. The kinetic curves are remarkably non-linear against log(t). Secondly, CRM acquisition is already observed at the low temperature of 175 °C, although it becomes measurable only after the comparatively long time interval t_{st} of ∼7 hr. The value of t_{st} decreases quickly with increasing T_{CRM}; above 300 °C CRM formation is 'instantaneous', i.e. t_{st} is shorter than the time span before the first CRM measurement can technically be taken. Thirdly, the CRM(t) curves observed for $T_{CRM} = 200$ and 225 °C and—quite likely—for 235 °C as well, are remarkable in the sense that they show an intermediate peak in the initial part of the curve. We interpret this

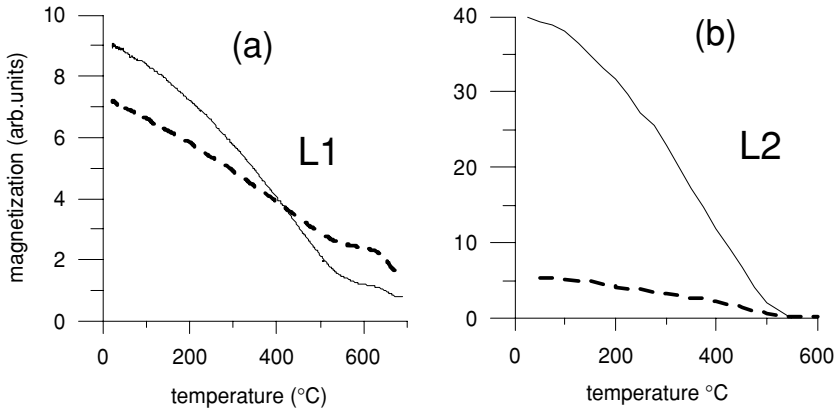

Figure 4. Strong-field thermomagnetic curves of bulk samples L1 and L2 pre-heated at 700 °C and 600 °C respectively (VSM, UIPE Moscow). The full lines refer to the heating curves of the first thermomagnetic run (equivalent to a second heating). The dashed lines indicate a repeat thermomagnetic experiment (equivalent to a third heating).

phenomenon as indication for a two-stage maghemite formation process as discussed above. The time t_1 after which the intermediate peak is reached decreases with increasing T_{CRM}. Note that the two-stage process is hinted at in the 250 and 275 °C CRM(t) curves as a change in the slope of the initial parts of the curves. From 275 °C upwards the CRM(t) curves are symmetric indicating the formation of high-temperature maghemite (type B) only.

The CRM intensities (measured at T_{CRM} and at T_r) against the annealing temperature T_{CRM} are plotted for both the 2.5 hr runs (Fig. 6a) and the 500 hr runs (Fig. 6b). The susceptibility at room temperature was measured for the samples of the 2.5 hr runs and plotted versus T_{CRM} (asterisks in Fig. 6a). The hysteresis parameters M_s, M_{rs}, the coercive force H_c, remanence coercive force H_{cr} and the ratios of M_{rs}/M_s and H_{cr}/H_c were also obtained for these two sets of experiments at T_r (Figs 6c–h). The temperature dependence of the CRM intensities (measured at T_{CRM} and T_r) was similar in each set of experiments. The corresponding room-temperature values are evidently higher because of the increase in M_s with decreasing temperature. So, for the sake of simplicity, in the following we will consider the room-temperature results only.

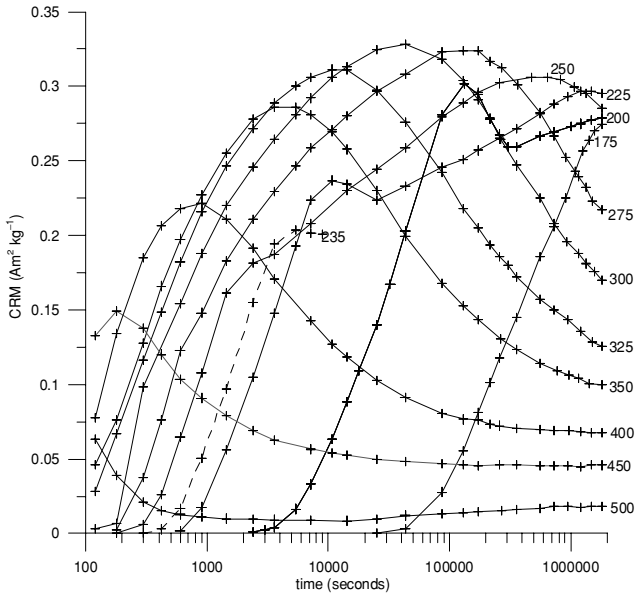

Figure 5. CRM intensity versus time (logarithmic scale) monitored at the temperature of CRM acquisition. The numbers near the curves refer to this acquisition temperature (T_{CRM}). The plus symbols show the actual experimental data points.

CRM intensity values plotted versus T_{CRM} in both sets yield asymmetrical peak-shaped curves, with a sharp increase in intensity with increasing T_{CRM} at low temperatures. After a local maximum, a minor decrease occurs with an intermediate minimum at about 200–235 °C. At yet higher T_{CRM} the CRM values reach a more pronounced maximum with a subsequent decrease to zero at 550 °C. The intermediate minimum is less pronounced for the 500 hr run and all maxima in the CRM(T_{CRM}) curves are shifted to lower temperatures in comparison with those of 2.5 hr runs (175, 250 ° and 225, 325 °C, respectively). Accordingly, the temperatures at which the CRM decrease slows down (Figs 6a and b) are also shifted to lower temperatures: to 325 and 400 °C for 500 and 2.5 hr of annealing time, respectively. The shift of the maxima together with the weakened intermediate minimum fit well to what is seen on the CRM versus time curves (Fig. 5): kinetic aspects play an essential role. Moreover the difference in behaviour of CRM(T_{CRM}) between two sets shows that CRM acquired by the first type of maghemite (A) was probably partly destroyed during prolonged heating. So, type A maghemite is not a stable phase. Thus, the CRM intensity as a function of T_{CRM} shows a double-peak pattern similar to what was found by Özdemir & Dunlop (1993). Their synthetic acicular lepidocrocite had an elongation factor of about 13–30. The annealing time in their experiments was 2.5 hr. A noticeable difference between the present results and those of Özdemir & Dunlop (1993) is the expression of the 'intermediate' minimum of CRM(T_{CRM}), which is only about 10 per cent of the CRM maximum value in our case but amounts to 90 per cent in the data of Özdemir & Dunlop (1993).

It is noteworthy that the behaviour of the susceptibility versus T_{CRM} differs significantly from that of the CRM intensity in the 2.5 hr set of experiments. The susceptibility experiences a single maximum at a temperature T_{CRM} of 235 °C where the CRM intensity has a local minimum. Further, the susceptibility decreases linearly by about 35 per cent over the same temperature interval where CRM increases. It stays almost constant over the interval of the main CRM intensity peak. Similar differences in the behaviour of CRM and susceptibility, reflected in distinct shifts between their maxima, were observed by McClelland & Goss (1993) in their experiments with lepidocrocite, annealed for 20 min in the temperature interval from 100 to 664 °C. They found, by control experiments determining

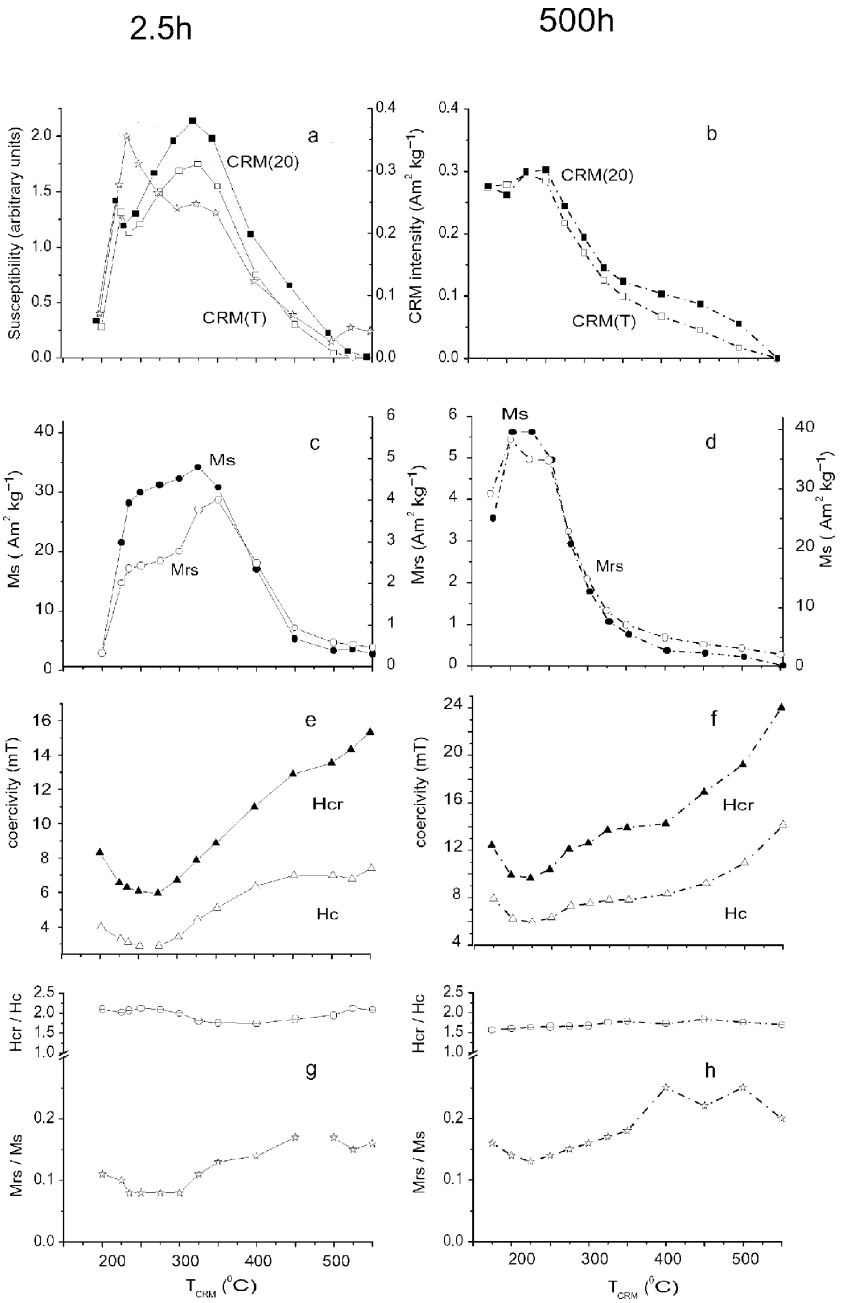

Figure 6. Natural lepidocrocite Lnd. Main rock magnetic behaviour as a function of the CRM acquisition temperature for annealing times of 2.5 hr (left-hand panels, full lines) and of 500 hr (right-hand panels, dash-dotted lines). (a, b) CRM intensities taken at the acquisition temperature (open squares), CRM intensities at room temperature after cooling in a zero field (full squares), AC susceptibility at room temperature (open stars). The other rock magnetic parameters were determined on samples that were cooled to room temperature as well. (c, d) Saturation magnetization M_s (full circles) and remanent saturation magnetization M_{rs} (open circles) as function of CRM acquisition temperature. (e, f) Coercive force H_c (open triangles) and remanent coercive force H_{cr} (full triangles). (g, h) Remanence ratio M_{rs}/M_s (open stars) and coercivity ratio H_{cr}/H_c (open circles) as a function of CRM acquisition temperature.

the mass loss, that the susceptibility began to decrease before all lepidocrocite has dehydroxylated to maghemite.

4.3.1 Temperature dependence of M_s and M_{rs}

M_s values continue to increase smoothly throughout the temperature interval of 235–325 °C (Fig. 6c), in which the susceptibility decreases (compare Figs 6a and c). The CRM values measured at T_r correlate reasonably well with the corresponding values of $M_s(T_{CRM})$; the latter curves display no intermediate minimum. Thus, the CRM intensity is controlled mainly by the maghemite content for annealing temperatures up to 400 °C. Variations in maghemite grain size are apparently of lesser importance. The sharp decrease of the $M_s(T_{CRM})$ values after 375 and 250 °C in the 2.5 and 500 hr runs respectively (Figs 6c, d) may conveniently be explained by the mere transformation of maghemite into haematite. The difference between $M_s(T_{CRM})$ curves for the 2.5 and 500 hr runs is not only apparent from the shift of the maxima but also from the width of these curves, referred to as the 'median destructive temperature' (MDT). MDT decreases about 1.5 times when the annealing time

is increased from 2.5 to 500 hr. Formally the $M_s(T_{CRM})$ curve for the 2.5 hr run can be described by the sum of two peaks, i.e. components with different widths similar to the $M_s(T)$ curves shown in Fig. 1. The $M_s(T_{CRM})$ curve for the 500 hr run looks more like a single-peak curve. This is also connected to the suppression of the first reaction stage during prolonged heating. Maghemite transforms more quickly (i.e. at a lower temperature) to haematite with longer annealing time: after their maxima M_s values drop more rapidly for the 500 hr runs (compare Figs 6c and d).

Maximum M_s values of about 34–39 A m^2 kg^{-1} found for both sets are well below the nominal maghemite saturation magnetization value of 77 A m^2 kg^{-1} (Bate 1980). For maghemite formed from lepidocrocite reported M_s values are 15.7 A m^2 kg^{-1} (Sakash & Solntseva 1971) and 39.7 A m^2 kg^{-1} (Özdemir & Dunlop 1993). The latter value is very close to the range obtained here. It could be that maghemite is already partially transformed to haematite before all lepidocrocite has been reacted but reduced M_s values are often reported for maghemites of different origin and grain size (see also Section 5.2).

The saturation remanent magnetization curve $M_{rs}(T_{CRM})$ for the set of 2.5 hr runs (Fig. 6c) is more similar to the CRM(T_{CRM}) dependence than to the $M_s(T_{CRM})$ behaviour. It shows an increase with temperature, first followed by a flat and poorly resolved maximum in the same temperature interval as the susceptibility maximum (and the 'intermediate' CRM minimum). After that, a second sharp maximum is observed followed by a decrease concurring with the behaviour of M_s and CRM intensity. Therefore, in the two-stage process of maghemite formation both saturation magnetization and CRM are connected to the same grain ensemble. For the 500 hr runs, however, the M_{rs} and M_s curves versus T_{CRM} look quite similar. A peak-type dependence of the saturation magnetization on T_{CRM} as observed here is not reported by Özdemir & Dunlop (1993) who documented fairly constant M_s values in runs from 220–550 °C and decreasing M_s values after their 615–653 °C runs. It could well be that those differences are related to differences in grain size and shape of the starting lepidocrocite in both studies.

The M_{rs}/M_s ratios (Figs 6g and h; lowermost curves) vary between 0.08 and 0.15 for the 2.5 hr runs and between 0.12 and 0.22 for the 500 hr runs. This ratio demonstrates a wide minimum over the same temperature intervals as the coercivity (*cf.* Section 4.3.2). The reduction in M_{rs}/M_s from the theoretical value 0.87 or 0.5 for SD particles of different shape (Gans 1932; Stoner & Wolfarth 1948) can be attributed to the presence of a superparamagnetic component in the samples throughout the whole temperature interval 175–550 °C. This markedly differs from data from Özdemir & Dunlop (1993) who observed a sharp increase inM_{rs}/M_s from 0 to 0.37 after runs at 150–225 °C followed by almost constant values up to 615 °C. This difference may be explained by higher grain sizes of both the initial lepidocrocite and the maghemite forming from it.

4.3.2 Temperature dependence of H_c and H_{cr} and median destructive fields

H_c and H_{cr} first drop to a minimum with increasing annealing temperature, then they increase with a variable rate for different temperature ranges (Figs 6e, f). The coercivity minima (for H_c: ∼3 and ∼6 mT after 2.5 and 500 hr annealing; corresponding H_{cr} minima: ∼6 and ∼10 mT) are observed in the same temperature interval as the local minimum of the CRM(T_{CRM}) curve. Both H_c and H_{cr} show an approximate two-fold increase at 550 °C. The H_{cr}/H_c values lie between 1.8 and 2.1 and 1.6and 1.8 for the 2.5 and 500 hr runs, respectively (Figs 6g, h), higher than the theoretical SD values

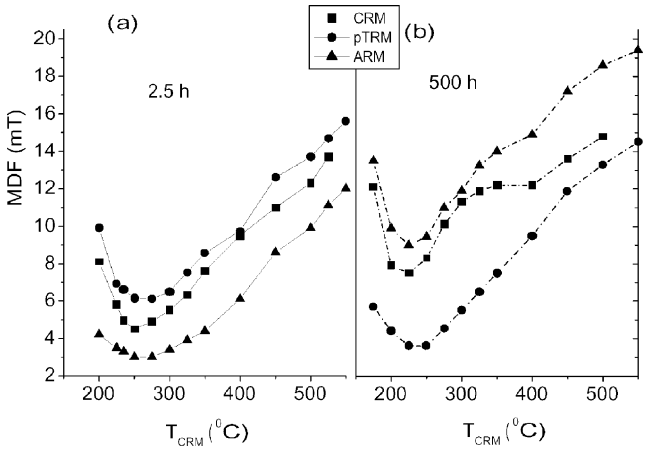

Figure 7. Median destructive fields of CRM (filled squares), ARM (filled triangles) and pTRM (filled circles) as a function of CRM acquisition temperature for 2.5 hr annealing (left panel, full lines) and 500 hr annealing (right panel, dash-dotted lines).

of 1.04–1.09 (Stoner & Wolfarth 1948), pointing to the presence of SP particles in the samples (Bean & Livingstone 1959; Kneller & Luborsky 1963; Roberts *et al.* 1995; Dunlop & Özdemir 1997). H_{cr}/H_c values for the 500 hr runs show a gradual shift to pseudo-single-domain (PSD) values with increasing annealing temperature.

The CRMs were demagnetized in an alternating field (AF) at room temperature. Subsequently, an anhysteretic remanent magnetization (ARM) and a pTRM were AF demagnetized as well. Median destructive field (MDF) values of these remanences are shown in Fig. 7. They show a similar behaviour as a function of annealing temperature as the coercivities. The CRM MDF values are significantly lower than those of Özdemir & Dunlop (1993), who observed an almost continuous MDF increase from 10 to about 20 mT after runs at 300–555 °C. It may be possible that they could have measured only the increase of MDF with temperature because of low levels of remanent magnetization.

Bagin *et al.* (1971) found a coercivity behaviour similar to that reported here. However, the present behaviour noticeably differs from that reported by Özdemir & Dunlop (1993). They observed a sharp increase in both H_c (from 0 to 10 mT) and H_{cr} (from 7 to 13 mT) between 200 and 250 °C, then a slower rise over the interval 250–600 °C up to 12 and 18 mT, respectively. It should be noted that CRM in their experiments became measurable after 225 °C only and coercivity measurements were started after the 200 °C run when $H_c = 0$. They explained this result by arguing for formation of 75 per cent stable SD particles and 25 per cent of SP particles. Indeed, such values seem to be rather low for maghemite SD particles, although a wide variety of both theoretical and experimental values are found in the literature (see review by De Boer 1999). H_c values for fine elongated SD maghemite particles ranged from 23 to 36 mT and from 7.5 to 15 mT for equidimensional fine particles (see review in Özdemir & Dunlop 1988). Goss (1988) calculated that a coercivity of about 4 mT would correspond to 37 nm grains.

The coexistence of SP and SD grains may be traced by measuring hysteresis loops (e.g. Tauxe *et al.* 1996). Indeed, we found that the loops taken after 2.5 hr annealing at $T \leq 450$ °C display such behaviour (Fig. 8). It is noteworthy that after the sample was heated to 580 °C, the constriction of the loop became much less noticeable, leading to a substantial increase in the coercivity and a decrease of intensity of magnetization, evidently due to the transformation

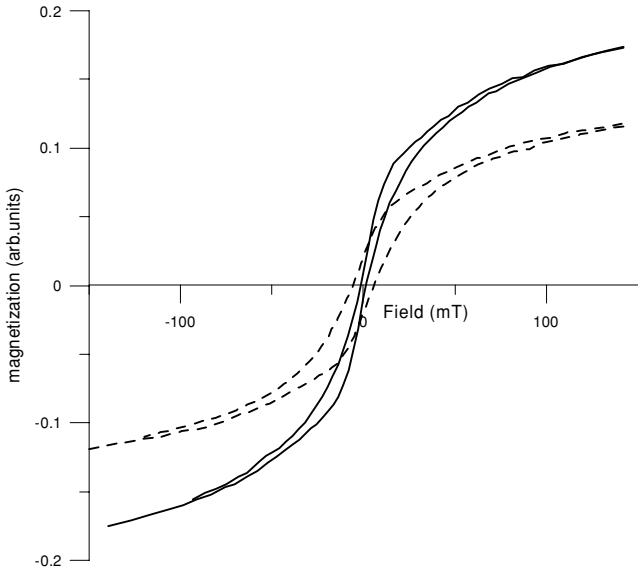

Figure 8. The central parts of the hysteresis loops acquired at room temperature for a sample annealed for 2.5 hr at 275 °C showing clearly the wasp-waistedness (full lines) with a hysteresis loop acquired after subsequent annealing at 580 °C, no longer showing wasp-waistedness (dashed lines).

of SP maghemite grains to SD maghemite and finally to haematite particles.

The magnetic softening, minima in CRM intensity with the corresponding maxima in susceptibility, could be made plausible by an increase in the relative proportion of superparamagnetic grains. Alternatively, structural changes in the maghemite could be proposed along the lines set out by Banfield *et al.* (1994) in a TEM and magnetic properties study of a natural magnetite/maghemite system. They provided an explanation for the softening of the maghemite with increasing annealing temperature up to 275 °C which may have relevance for the lepidocrocite–maghemite reaction reported on here. Their analysis of microstructures as a function of annealing temperature showed that a decrease in coercivity is related to the removal of stacking faults with $\langle \frac{1}{4}\frac{1}{4}0 \rangle$ displacement in the maghemite. Planar structures of width 0.6 nm subdivide non-heated maghemite grains formed in the laboratory into subgrains. After heating at 200 °C these planes were removed with a corresponding decrease in coercivity. Upon heating the lepidocrocite to low temperatures of 175–200 °C, slow dehydroxylation and the formation of the activated intermediate lepidocrocite as described by Gehring *et al.* (1990) occurs with the development of maghemite type A characterized by superstructures in the vacancy distribution (reported on in detail in a future paper). Also, stacking faults can occur dividing maghemite grains into subgrains. These stacking faults and also small, topotactically oriented residual amounts lepidocrocite, are envisaged to contribute to magnetic hardness. At higher annealing temperatures (225–275 °C, 2.5 hr annealing) the stacking faults as well as the lepidocrocite–maghemite boundaries would diminish, resulting in a decrease of coercivity, M_{rs}/M_s values and CRM intensity. Along the lines of Banfield *et al.* (1994), at higher temperatures more maghemite is formed without these stacking faults. Wasp-waisted loops can be explained as a consequence of small maghemite regions between the residual stacking faults. At temperatures higher than 275–300 °C the rate of lepidocrocite dehydroxylation is much higher. Maghemite type B then forms with a different vacancy distribution and new planar faults, which results in the increase of coercivity, CRM and M_{rs} (second maximum). By analogy with Banfield *et al.* (1994), most of the CRM in our samples is probably associated with structural defects in maghemite.

4.4 Thellier–Thellier experiments

Several Thellier–Thellier experiments with the CRM as the primary natural remanent magnetization (NRM) were carried out on Lnd samples in order to investigate the similarity of the Arai–Nagata plots to the TRM as the primary NRM. All CRM-TRM1 diagrams (TRM1 being the first laboratory TRM) show extremely concave-up plots as exemplified in Fig. 9a. For the second experiment, the same samples were given a second TRM, TRM2, acquired by cooling from 580 °C to room temperature in the same field. They were again subjected to the Thellier–Thellier procedure. Contrary to the previous case, these plots show a classic straight line with tangent very close to 1 up to 560 °C (Figs 9a and b). This proves that no mineralogical changes are going on, at least during the second heating to 560 °C. Besides, the carriers of the TRM must be of SD size as only PSD and MD grains display concave-up plots (Shcherbakov *et al.* 1993). On further heating above 560 °C an unusual kink appears in Fig. 9(b), when the representative points start to move in the

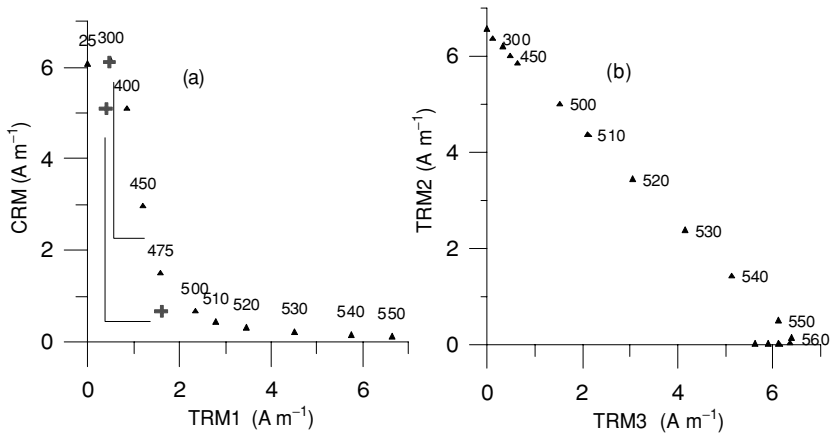

Figure 9. (a) Arai–Nagata plot for CRM obtained at a temperature of 350 °C for 8 hr annealing time. The plus symbols show the pTRM checks. (b) Arai–Nagata plot for TRM (TRM2) imparted after the completion of the Thellier–Thellier experiment with the CRM. The pTRM checks appear to coincide completely with the TRM2–TRM3 data point checks, therefore they are not shown.

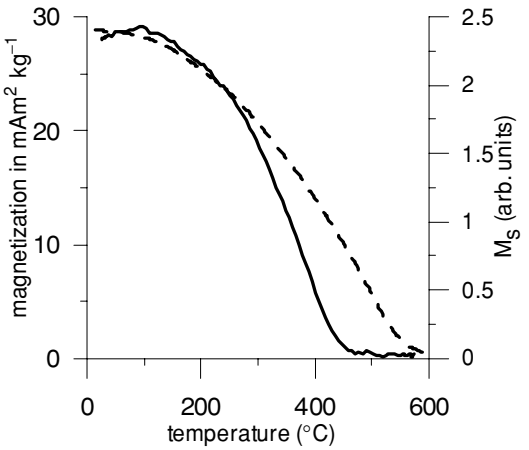

Figure 10. Continuous thermal demagnetization of CRM acquired during annealing a lepidocrocite sample at $T = 350$ °C for 8 hr (full line). The behaviour of the saturation magnetization M_s of the same sample is shown with the dashed line.

opposite sense, evidently due to the transformation of maghemite to haematite.

Fig. 10 displays the thermal demagnetization curve of the CRM together with the saturation magnetization of the same sample. The shape of the thermal demagnetization curve is in good agreement with the corresponding Arai–Nagata pattern (Fig. 9a), which also demonstrates a quick decay from 300 to 500 °C. The thermomagnetic curve of the saturation magnetization confirms the conclusion of the previous sections that the carriers of CRM are maghemite grains with T_C of about 560 °C.

5 DISCUSSION

In this section four main aspects will be dealt with. First we discuss the apparently different temperatures of maghemite formation as following from different types of measurement. Ways to determine the amount of maghemite present, its Curie temperature and its thermal stability form the second topic. Then, CRM versus time-dependent properties will be analysed and finally the implications of the Thellier–Thellier experiments will be evaluated.

5.1 Apparently different starting temperatures of the lepidocrocite transformation and temperature–time considerations of the reaction chain

From the strong-field thermomagnetic curves (Fig. 1) it follows that the generation of maghemite starts at $T_{st} \approx 250$ °C, except in the case of poorly crystalline lepidocrocite which starts to alter at ~200 °C. The $k(T)$ curve, however, so indicative of the presence of maghemite, starts to rise later around 300 °C (Fig. 2). $k(T)$ values mainly reflect the temperature variation of the susceptibility of SP grains, while the saturation magnetization $M_s(T) = I_s(T)w$ is proportional to the maghemite content. Here I_s is the spontaneous magnetization of the magnetic phase expressed on a mass-specific basis and w is the relative weight content of maghemite (compared with the sample mass). During the initial stage of the transformations, w increases rapidly with T which, in turn, leads to the sharp increase in M_s.

On the other hand, the AC in-phase susceptibility, measured at the frequency ω, is (Worm & Jackson 1999):

$$k(\omega, T) = \left(\frac{I_s^2 v^2 n}{3k_B T}\right)\left(\frac{1}{1+\omega^2\tau^2}\right). \quad (3)$$

Here n is the number of grains with volume v expressed per unit volume of the sample, τ is the relaxation time of the grains and v is volume. Hence, the AC susceptibility is determined mainly by the SP grains that satisfy the condition $\omega\tau \ll 1$. Taking into account that the relative volume concentration $c = nv$ and $w = cP_m$ where P_m is the specific gravity of maghemite, we get instead of (3):

$$k(\omega, T) = \left(\frac{I_s(T)M_s(T)v}{3k_B T P_m}\right)\left(\frac{1}{1+\omega^2\tau^2}\right). \quad (4)$$

Thus, the AC susceptibility is proportional to the product of M_s and the volume v. So, a plausible explanation for the delay in growth of k is that during the very first stage of the transformation at $T > T_{st}$ massive nucleation of very small maghemite particles (or small regions of planar defects) would take place, reflected in a sharp increase of M_s. These particles continue to grow in volume at higher temperature (or the planar defects decrease with a concurrent increase in size of the maghemite regions) and this is reflected in the increase of $k(T)$ dependence. When the temperature increases to about 350–370 °C, the volume of the grains reaches a value determined by the condition that the relaxation time τ approaches $1/\omega$. From eq. (4) with $E_B = Kv$, (E_B = magnetic blocking energy; K = anisotropy constant; v = grain value) it follows that the AC susceptibility reaches its maximum due to increasing volume in this temperature range. Consequently, on further heating $k(T)$ decreases rapidly due to both the blocking of the SP grains (formally it follows from the inequality $\omega\,\tau > 1$) and the inversion of maghemite to haematite.

In contrast to the $M_s(T)$ and $k(T)$ experiments, the monitoring of CRM acquisition shows that CRM is already detectable on the Lnd sample at 175 °C annealing. However, it took 7 hr of annealing before the remanence was developed (Fig. 5). Obviously, this reflects the dependence of the degree of lepidocrocite transformation on the heating rate (or the time of annealing): the slower the heating (or the longer the annealing time), the earlier is the appearance of maghemite and its subsequent inversion to haematite. It should be recalled that a minimum temperature is required: Sakash & Solntseva (1971) did not observe any structural change in lepidocrocite annealed at 105 °C for 227 hr and Gehring & Hofmeister (1994) pointed out that the lepidocrocite δ-OH bands started to weaken after heating at just 176 °C.

To further illustrate this, Fig. 11 shows the combination of the two normalized $M_s(T_{CRM})$ curves (from Fig. 6) obtained for 2.5 and 500 hr annealing time with the similar curve of $M_s(T)$ taken from Fig. 1(d) (also normalized). Remember that the last curve was obtained during continuous heating of the sample, so it was recalculated to $T = T_r$ according to the relationship $M_s(T_{CRM}) = M_s(T)(I_s(T_r)/I_s(T))$ to make all curves comparable to each other. The required temperature behaviour of $I_s(T)$ was taken from the cooling curve (Fig. 3). The resulting curves are similar to each other but shifted on the temperature axis (Fig. 11). This demonstrates the strong tendency of the lepidocrocite–maghemite transformation to shift to lower temperatures when the time available for the reaction is increasing. This gives the possibility to extrapolate the experimental results acquired on a laboratory timescale to processes taking place on natural timescale (see Section 5.3).

The same can be stated for the transformation rate of maghemite to haematite, also apparent from Fig. 11. Thus, this study once more provides evidence that it is not the temperature alone but the temperature–time combination that is responsible for the acquisition or decay of a magnetic remanence during a solid phase reaction. For example, the so-called 'inversion temperature' of the maghemite to haematite transition is reported to vary from 350 to 650 °C. Morrish

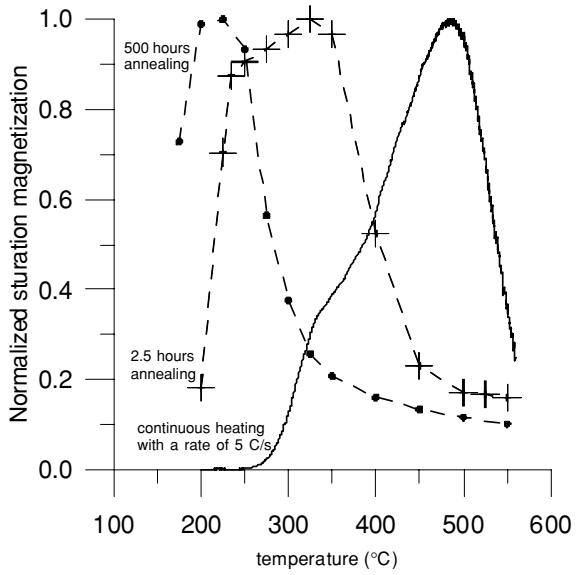

Figure 11. Dashed lines: saturation magnetization measured at room temperature (normalized to maximum values) versus CRM acquisition temperature for Lnd lepidocrocite (same data as shown in Fig. 6). The full circles indicate the experimental data points for 500 hr annealing time, the plus symbols indicate those for 2.5 hr annealing time. The full line shows the temperature-dependent behaviour of the saturation magnetization of Lnd lepidocrocite during continuous heating (same data as in Fig. 1d), normalized to its maximum value and recalculated to values at room temperature to make it comparable to the other two curves shown.

& Sawatsky (1971), Ozima & Ozima (1972) and Housden *et al.* (1990) suggested that the inversion is a thermally activated process. Therefore, the inversion temperature depends on the timescale over which inversion is allowed to take place; this is millions of years in nature (Adnan & O'Reilly 1999). Also, the amount and type of maghemite that is formed varies with the rate of dehydroxylation of lepidocrocite (see Figs 1c and d).

5.2 Maghemite amount, Curie temperature, thermal stability and vacancy ordering

The relative weight w of maghemite in a sample is of prime importance for assessing the (relative) maghemite content during a thermal experiment. Hence, measurement of an $M_s(T)$ curve allows us to estimate $w = M_s(T)/I_s(T)$, provided that we know the $I_s(T)$ dependence. Dunlop & Özdemir (1997) recommend the use of $I_s(T_r) = 78$ A m^2 kg^{-1} for maghemite. However, for fine grains, which make up the main subject of this study, $I_s(T_r)$ can be substantially lower (Coey & Khalafalla 1972; Goss 1988; Novakova *et al.* 1992; Han *et al.* 1994; De Boer & Dekkers 2001). Various mechanisms have been postulated to explain the decrease in saturation magnetization with particle size: a non-magnetic surface layer of width ~0.6 nm (Berkowitz *et al.* 1968), absorbed water, a non-collinear spin arrangement (Coey & Khalafalla 1972) and variations in vacancy concentration on the B and A sites in the spinel lattice (Goss 1988; De Bakker *et al.* 1991). The reported $M_s(T_r)$ values for fine maghemite grains of different origin ranging from 43 to 5 nm are 16–66 A m^2 kg^{-1} (Han *et al.* 1994; Novakova *et al.* 1992).

The results presented in Fig. 6 give ~40 A m^2 kg^{-1} as the lower limit of the I_s values for the Lnd samples at room temperature. Let us take a $I_s(T_r)$ of 50 A m^2 kg^{-1}, i.e. somewhat higher to avoid extreme cases. The temperature behaviour of $I_s(T)$ follows again from the cooling curve (Fig. 3), the corresponding $w(T)$ dependence is also shown in the same figure. Because I_s as function of T does not change significantly until T is far from T_c, the curves of $M_s(T)$ (during the first heating) and $w(T)$ correlate with each other, with the exception that the maximum maghemite content is shifted to a higher temperature of ≈450 °C. At that temperature the maghemite content amounts to ~60 per cent, the remaining 40 per cent should be attributed to haematite as the lepidocrocite can hardly survive at this temperature. As a cautionary note: the actual values of $w(T)$ should not be taken too strictly because of the approximations made in the above.

The Curie temperature of the maghemite surviving the first heating to 600 or 700 °C is estimated to be 500–570 °C (Figs 3 and 4) which is substantially less than the value of 645 °C quoted by Dunlop & Özdemir (1997). However, it is close to a T_C of 848 K (575 °C) estimated by extrapolation of x to $x = 0$ in $(FeO)_xFe_2O_3$ (Neél 1949). Also Aharoni *et al.* (1962) obtained a value of 860 K (587 °C) for T_C and Rybak (1971) determined T_C at 570 °C for well-defined maghemite. The value of $T_C < 600$ °C is also supported by measurements of the $M_s(T)$ dependence for the samples subjected to CRM experiments (Figs 3 and 12a). The lowering of the Curie point is consistent with the common opinion that T_C may be significantly reduced in fine grains and thin films due to the influence of surface phenomena and tetragonal symmetry (Barinov 1982; Babkin *et al.* 1991) and the disordering of the vacancy distribution (Takei & Chiba 1966; De Boer & Dekkers 2001; Liu *et al.* 2003).

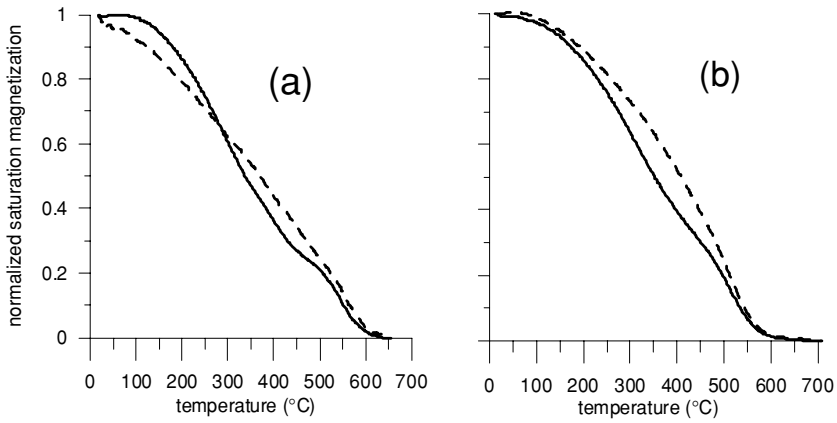

Figure 12. Normalized thermomagnetic curves $M_s(T)$ for Lnd samples subjected to annealing: (a) for 2.5 hr at $T = 225$ °C (full line) and at $T = 500$ °C (dashed line); (b) at $T = 275$ °C for 2.5 hr (full line) and for 500 hr (dashed line).

Takei & Chiba (1966) implied by 'disordered' a random vacancy distribution over both tetrahedral and octahedral sites.

In addition to being able to determine the Curie point, the $M_s(T)$ curves nicely show the evolution of the maghemite phase (or phases) with annealing temperature (Fig. 12a) or annealing time (Fig. 12b): with less pre-treatment (full lines), more intermediate phases develop during the heating. Indeed, the full lines show the presence of an inflection point which, in our opinion, indicates the transition of the less stable maghemite A phase into more stable B maghemite and possibly haematite. For the 225 °C annealing (2.5 hr) the inflection point lies at ∼300 °C (Fig. 12a) and for the 275 °C annealing (2.5 hr) at ∼350 °C (Fig. 12b). Note, that Banfield *et al.* (1994) observed about 80 per cent demagnetization of NRM residing in maghemite after heating at 300 °C without any traces of a γ- to α-Fe_2O_3 transition. They explained this by the removal of structural defects.

The dehydroxylation of residual lepidocrocite to maghemite after the 225 °C run also contributes to the convex part of the thermomagnetic curve in Fig. 12(a). This follows from the peak-shaped thermomagnetic curve after the 200 °C run (not shown in Fig. 12a). Further heating of this sample for 1 hr at 350 °C demonstrated a smooth rise of M_s pointing to an ongoing process of maghemite formation. The less stable intermediate maghemite phase is observed in thermomagnetic curves of samples heated for 2.5 hr at 225–275 °C. After heating at 350 °C the thermomagnetic curve looks single-phase and similar to that shown in Fig. 12(a) (dashed line). Note that the coercivity of material obtained during CRM experiments also increases after heating at 275 °C (Figs 6e, and 7), when the intermediate maghemite phase disappears (or stacking faults are eliminated), suggesting that less stable maghemite A is magnetically softer than more stable maghemite B. There are two possibilities for the transformation of maghemite A: the first is conversion into more stable maghemite B and the second is conversion of γ-Fe_2O_3 to α-Fe_2O_3. The presence of a small amount of haematite that would appear during the course of heating is difficult to evaluate from thermomagnetic curves because of its small concentration and in particular its low M_s value.

The existence of at least two metastable maghemites, a low- and a high-temperature form, during the course of oxidation of magnetite to haematite was proposed by Goss (1988). The first maghemite has a face-centred cubic lattice, the second a primitive cubic structure. Adnan & O'Reilly (1999) applied the common model of competing energy terms of the volume and surface contributions to the γ- to α-Fe_2O_3 transition when a small haematite nucleus appears within a non-inverted maghemite crystal. The combination of these two terms provides an energy barrier to the growth of the haematite inclusion. Only after the inclusion has grown beyond a critical radius R_{cr} may the remainder of the particle be rapidly transformed to the α-form. This model would explain the different temperatures of the γ- to α-Fe_2O_3 transition reported in the literature. Differences in the starting material, for instance concerning the surface area, particle size and/or shape, appear to be very important for the stabilization of maghemite grains. For example, Adnan & O'Reilly (1999) did not observe any decrease in saturation magnetization of maghemite being heated at 400 °C for 4 hr. Acicular maghemite converted to haematite on a laboratory timescale only after heating to 750 °C (Özdemir 1990). On the other hand, the conversion of spherical grains with a median grain size of 24.5 nm was completed between 500 and 600 °C (Özdemir & Dunlop 1988).

Maghemite particles convert to haematite forming nanoparticles, either as inclusions or as whole grains. Either way, the number of defects in the maghemite lattice is likely to increase. This leads to a reduction in the mobility of phase boundaries making the remainder of the maghemite more stable: Morrish & Sawatsky (1971) obtained an increase of 1.6 times for the activation energy of Co-doped maghemite (∼3 per cent Co) when compared with pure maghemite. The stabilization of maghemite may also be due to the inclusion of additional H^+ in the crystal structure (Aharoni *et al.* 1962). This last mechanism for the stabilization of maghemite nanoparticles seems most likely during lepidocrocite dehydroxylation. Indeed, it is reasonable to suggest that small maghemite grains lose additional water more easily than bigger ones; thus, they can be converted to haematite at quite moderate temperatures while the bigger grains (1–2 μm in size), which would be stabilized by the extra hydroxyl groups, still retain the maghemite structure.

In the present study we found three phases involved in the process of dehydroxylation of lepidocrocite: two maghemite types (an unstable A phase and a more stable B phase) and haematite. Undestroyed residual lepidocrocite appeared to still be present as well. Different maghemite phases might appear, since solid state reactions often lead to unusual effects because of the limited opportunity provided for atomic rearrangement. In particular, the formation of dehydrated phases is often pseudomorphic after their hydrated precursors (e.g. Ervin 1952). Hence, the formation of well-crystallized maghemite proceeds with complete or partial preservation of the original cation configuration through the generation of so-called semi-coherent interphase boundaries, a topic that will be expanded in a future paper. Takei & Chiba (1966) also reported that maghemite, prepared by calcination of lepidocrocite at low temperature, preserves the original cation configuration. As a result, vacancies were ordered in octahedral positions of the maghemite structure. Further annealing of the lepidocrocite for another 8 hr ends up with the almost entire disintegration of the parent lepidocrocite phase. The maghemite grains can now form their own structure which is not dictated by the parent lepidocrocite so the vacancy ordering may be lost. Two competing processes are envisaged to transform the originally ordered maghemite structure: disordering of vacancies on further annealing as well as haematite formation. Takei & Chiba (1966) reported on the decrease in intensity of superstructural maghemite lines on X-ray diffractograms along with the increase in annealing temperature.

5.3 Further aspects of the CRM acquisition

The CRM acquisition runs with $T_{CRM} \leq 300$ °C exhibit a substantial delay time t_{st} to the start of CRM acquisition. Dehydroxylation of the initial lepidocrocite material, a pre-condition for the formation of maghemite (Takei & Chiba 1966; Gehring & Hofmeister 1994), is thought to be the cause of this delay time in CRM acquisition. It progressively decreases with increasing annealing temperature. By extrapolation using Arrhenius' law (eq. 6) that describes reaction kinetics as function of temperature, we can estimate roughly the time t_{st} to achieve noticeable CRM acquisition at temperatures as low as the ambient temperature:

$$t_{st} = A \exp\left(\frac{E_B}{kT}\right) \quad \text{or} \quad \log(t_{st}) = \log A + \frac{E_B}{kT}. \tag{5}$$

By plotting $\log(t_{st})$ against $1/T$, one can estimate the parameters A and E_B and extrapolate from a certain temperature interval as shown by the open symbols in Fig. 13. Gehring & Hofmeister (1994) found that the dehydroxylation was completed over 48 hr run at 176 °C; however, it had not significantly proceeded after 1 hr annealing at the same temperature. These observations agree with our results for the 175 °C run when CRM formation started after 7 hr annealing. The M_s data (Figs 6c and d) also agree in general with these estimations as there was no detectable M_s value after the 2.5 hr run

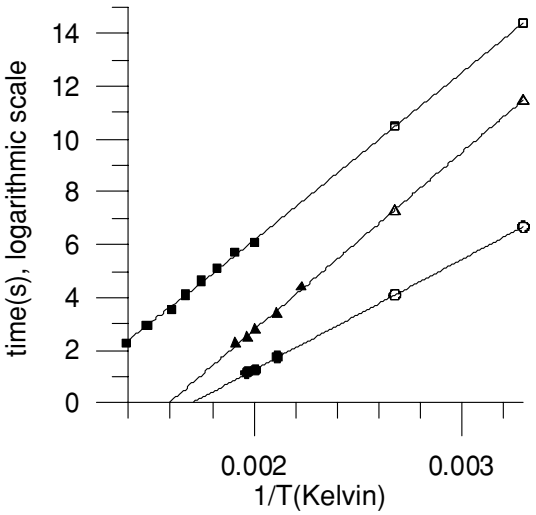

Figure 13. Values for the delay time t_{st} of CRM acquisition (full triangles), for the time t_1 of the initial lepidocrocite destruction (full circles), and for the time t_2 of the onset of the transformation from maghemite to haematite (full squares). The lines are linear fits to the data. For convenience extrapolated values of t_{st}, t_1 and t_2 to 100 and 30 °C are given by the open symbols to estimate the duration of the respective reactions at those temperatures.

at this temperature but a well measurable M_s appeared after 500 hr annealing.

An unusual feature of the kinetic CRM(t) curves at relatively low T_{CRM} is the appearance of an intermediate maximum at a certain time t_1. We argue that this maximum marks the transformation from A maghemite to B maghemite, or the time of the complete destruction of the initial lepidocrocite. The transformation from A maghemite to B maghemite is rapid. Therefore, the rate-determining step of the lepidocrocite destruction is primarily the dehydroxylation reaction. We only have three experimental t_1 values, marked with full circles in Fig. 13. Nevertheless, the fitted line predicts that the final destruction of the lepidocrocite requires less time than the dehydroxylation over the whole temperature interval, concurring with its rate-determining character. Both processes seem to be quick—according to the estimates they should be completed in less than 100 000 yr at ambient temperature. Soil lepidocrocites are indeed not considered to be long-term stable phases. When dealing with hydrothermally formed very large crystalline lepidocrocites that may contain other isomorphously substituted cations, the activation energy of the dehydroxylation reaction, as determined here, could be experimentally underestimated.

Further, the CRM(t) temperature runs with T_{CRM} ranging from 225 to 450 °C exhibit a maximum at a certain $t = t_2$, related to the beginning of the transformation of maghemite to haematite. The corresponding data are shown by the squares (Fig. 13) and fitted with the line in the same way as for the t_{st} fitting. This process appears to be the slowest compared with the other two. At ambient temperatures it would take tens of millions of years to complete the transformation, so in practice maghemite would survive forever.

5.4 Implications of the Thellier–Thellier experiments

The non-linearity of the Arai–Nagata diagrams demonstrates the low capacity to acquire pTRM during the subsequent heating, which is usually related to the multidomain structure of the grains (Shcherbakov & Shcherbakova 2001). However, in the case of CRM such behaviour is not related to the domain structure but accounts for chemical and structural transformations during the course of the Thellier–Thellier experiments. Another manifestation of such transformations is the appearance of an unusual kink on the Arai–Nagata diagram for the TRM—when the heating temperatures reach values $T > 550$ °C, the representative points start to move in an opposite sense, evidently due to the transformation of maghemite to haematite. Thus, these features of Arai–Nagata diagrams reported in an experimental set-up for the first time, might be a discriminatory test for secondary NRM related to maghemite.

6 CONCLUSIONS

The transformation of lepidocrocite via maghemite to haematite occurs in four partially overlapping stages. First, the dehydroxylation of the initial lepidocrocite takes place. This process is completed on laboratory timescales at temperatures from 150 to 200 °C, as follows from the Lnd data. At ambient temperatures it may take up to 100 000 yr. The ordered yet unstable maghemite A phase with planar defects is formed next. Grains (or regions divided by stacking faults) are very small, often superparamagnetic as indicated by wasp-waisted hysteresis loops. The next stage is characterized by the complete transformation of lepidocrocite into maghemite. This leads to the generation of poorly crystalline maghemite grains with a Curie temperature close to 570 °C (B maghemite phase). This two-stage generation of maghemite is a specific feature of lepidocrocite destruction. On further annealing these grains may 'heal', i.e. recrystallize to bigger grains. Finally, the maghemite entirely converts into haematite. The presence of lepidocrocite in sediments may be inferred from asymmetric and double-peaked M_s versus temperature curves.

CRM is acquired by the nucleation and growth of maghemite through the superparamagnetic threshold size. A remarkable aspect of CRM acquisition is that it resides in the ordered maghemite that is commonly reported as unstable, during the initial stage of its formation. On further heating above 250 °C (or annealing for a longer time at lower temperatures) this maghemite converts into a more stable disordered maghemite B phase with a Curie temperature of 500–570 °C. This phase appears to be quite stable to heating: in some cases it proves to be entirely stable to heating to 600 °C so it can serve as a possible CRM carrier in rocks. In fact, the existence of such thermally stable maghemite may be easily mistaken for the magnetite in common palaeomagnetic practice. The corresponding NRM may be regarded as a TRM or a detrital remanent magnetization when dealing with sediments while it is, in fact, a CRM.

ACKNOWLEDGMENTS

This study was supported by INTAS with the project title 'An assessment of the ability of continental red beds to provide reliable information about geo-dynamic and geomagnetic earth history, using palaeomagnetic and rock magnetic methods' (grant number 99-1273). We appreciate the comments of two GJI reviewers.

REFERENCES

Adnan, J. & O'Reilly, W., 1999. The transformation of γ-Fe_2O_3 to α-Fe_2O_3: thermal activation and the effect of elevated pressure, *Phys. Earth planet. Inter.,* **110,** 43–50.

Aharoni, A., Frei, E.H. & Shiber, M., 1962. Some properties of γ-Fe_2O_3 obtained by hydrogen reduction of α-Fe_2O_3, *J. Phys. Chem. Solids,* **23,** 545–554.

Annersten, H. & Hafner, S.S., 1973. Vacancy distribution in synthetic spinels of seria Fe_3O_4–γ-Fe_2O_3, *Z. Kristallogr.,* **137,** 321–340.

Araki, H., 1989. Micro area X-ray diffraction techniques, *Rigaku J.,* **6**(2), 34–42.

Babkin, E.V., Koval, K.P. & Pynko, V.G., 1991. Magnetic properties of ferrimagnetic iron oxide gamma-Fe_2O_3 (in Russian), *Zh. Eksp. Teor. Fiz.,* **100**(2), 582–589 (translated in *ZhETP*, **73,** 321–325).

Bagin, V.I., 1967. The chemical remanent magnetization at temperature transitions of lepidocrocite and goethite (in Russian), *Izv. Akad. Nauk USSR, Fiz. Zem.,* **2,** 104–108.

Bagin, V.I., Gendler, T.S., Kuzmin, R.N. & Rybak, R.S., 1971. Study of magnetic properties and Mössbauer effect at temperature transition of siderite (in Russian), *Izv. Akad. Nauk USSR, Fiz. Zem.,* **11,** 71–84.

Banfield, J.F., Wasilelewski, P.J. & Veblen, D.R., 1994. TEM study of relationships between the microstructures and magnetic properties of strongly magnetized magnetite and maghemite, *Am. Mineral.,* **79,** 654–667.

Barinov, G.I., 1982. The influence of anisotropy on remanent direction of thin single crystal layers of iron oxides, *Geomagn. Aeron.,* **5,** 890–891.

Bate, G., 1980. Recording materials, in *Ferromagnetic Materials,* Vol. 2, pp. 381–507, ed. Wohlfarth, E.P., North Holland, Amsterdam.

Bean, C.P. & Livingstone, J.D., 1959. Superparamagnetism, *J. Appl. Phys.,* **30,** 120S–129S.

Berkowitz, A.E., Schuele, W.J. & Flanders, P.J., 1968. Influence of crystallite size on the magnetic properties of acicular γ-Fe_2O_3 particles, *J. Appl. Phys.,* **39,** 1261–1263.

Bernal, J.D., Dasgupta, D.R. & Mackay, A.L., 1957. Oriented transformation in iron oxides and hydroxides, *Nature,* **180,** 645–647.

Berry, F.J. & Helgason, O., 2000. Mössbauer spectroscopic properties of tin-doped iron oxides, *Hyperfine Interact.,* **126,** 269–275.

Brown, B.P., 1952. A superstructure in spinels, *Nature,* **170,** 1123.

Chuhrov, V.F. *et al*., 1975a. Experimental data on the conditions of iron oxides formation (in Russian), in *Hypergenic Fe-oxides,* pp. 11–33, ed. Petrovskaya, N.V., Nauka, Moscow.

Chuhrov, V.F., Zvyagin, B.B., Ermilova, L.P. & Gorshkov, A.I., 1975b. Formation and transformation of lepidocrocite (in Russian), in *Hypergenic Fe-oxides,* pp. 48–61, ed. Petrovskaya, N.V., Nauka, Moscow.

Coey, J.M.D. & Khalafalla, D., 1972. Superparamagnetic γ-Fe_2O_3, *Phys. Status Solidi (a),* **11,** 229–241.

Cornell, R.M. & Schwertmann, U., 1996. *The Iron Oxides,* VCH, Weinheim.

De Bakker, P.M.A., De Grave, E., Vandenberghe, R.E., Bowen, L.H., Pollard, R.J. & Persoons, R.M., 1991. Mössbauer study of the thermal decomposition of lepidocrocite and characterization of the decomposition products, *Phys. Chem. Miner.,* **18,** 131–143.

De Boer, C.B., 1999. Rock-magnetic studies on hematite, maghemite and combustion-metamorphic rocks—the quest to understand the hidden attraction of rocks, *PhD thesis,* Utrecht University (*Geologica Ultraiectina*, **177**).

De Boer, C.B. & Dekkers, M.J., 1996. Grain-size dependence of the rock magnetic properties for natural maghemite, *Geophys. Res. Lett.,* **23,** 2815–2818.

De Boer, C.B. & Dekkers, M.J., 2001. Unusual thermomagnetic behaviour of haematites: neoformation of a highly magnetic spinel phase on heating in air, *Geophys. J. Int.,* **144,** 481–494.

De Grave, E., Persoons, R.M., Chambaere, D.G., Vandenberghe, R.E. & Bowen, L.H., 1986. An ^{57}Fe Mössbauer effect study of poorly crystalline γ-FeOOH, *Phys. Chem. Miner.,* **13,** 61–67.

Dunlop, D.J. & Özdemir, Ö., 1997. *Rock Magnetism: Fundamentals and Frontiers,* Cambridge University Press, Cambridge.

Ervin, G., 1952. Structural interpretation of the diaspore—corundum and boehmite—γ-Al_2O_3 transition, *Acta Crystallogr.,* **5,** 103–108.

Ewing, F.G., 1935. The crystal structure of lepidocrocite, *J. Chem. Phys.,* **3,** 420–424.

Feitknecht, W. & Mannweiler, U., 1967. Der Mechanismus der Umwandlung von γ- zu α-Eisensesquioxid, *Helv. Chim. Acta,* **50,** 570–581.

Gans, V.R., 1932. Über das magnetishe Verhalten isotroper Ferromagnetika, *Ann. Phys., Leipzig,* **15,** 28.

Gehring, A.U. & Hofmeister, A.M., 1994. The transformation of lepidocrocite heating: a magnetic and spectroscopic study, *Clays Clay Miner.,* **42,** 409–415.

Gehring, A.U., Karthein, R. & Reller, A., 1990. Activated state in the lepidocrocite structure during thermal treatment, *Naturwissenschaften,* **77,** 177–179.

Gendler, T.S., Bagin, V.I., Butuzova, G.Yu. & Haliulina, E.A., 1999. The peculiarities of formation of Fe-Mn minerals from Tetis deep: data of magnetic mineralogy and Mossbauer spectroscopy (in Russian), in *Paleomagnetism and Rock Magnetism,* pp. 18–19, ed. Scsherbakov V.P., UIPE RAS, Moscow.

Giovanoli, R. & Brütsch, R., 1975. Kinetics and mechanisms of the dehydration of γ-FeOOH, *Thermochim. Acta,* **13,** 15–36.

Goss, C.J., 1988. Saturation magnetization, coercivity and lattice parameter changes in the system Fe_3O_4–γ Fe_2O_3 and their relationship to structure, *Phys. Chem. Miner.,* **16,** 164–171.

Haigh, G., 1958. The process of magnetization by chemical change, *Phil. Mag.,* **3,** 267–286.

Han, D.H., Wang, J.P. & Luo, H.L., 1994. Crystallite size effect on saturation magnetization of fine ferromagnetic particles, *J. Magn. Magn. Mater.,* **136,** 176–182.

Hedley, I.G., 1968. Chemical remanent magnetization of the FeOOH, Fe_2O_3 system, *Phys. Earth planet. Inter.,* **1,** 103–121.

Heider, F. & Dunlop, D.J., 1987. Two types of chemical remanent magnetization during oxidation of magnetite, *Phys. Earth planet. Inter.,* **46,** 24–45.

Housden, J., Desa, A. & O'Reilly, W., 1990. The magnetic balance and its application to studying the magnetic mineralogy of igneous rocks, *J. Geomagn. Geoelectr.,* **40,** 63–75.

Imaoka, Y., 1968. On the coercive force of magnetic iron oxides, *J. Electrochem. Soc. Japan,* **36,** 15–22.

Kneller, E.F. & Luborsky, F.E., 1963. Particle size dependence of coercivity and remanence of single-domain particles, *J. Appl. Phys.,* **34,** 656–658.

Kobayashi, K., 1961. An experimental demonstration of CRM with Cu-Co alloy, *J. Geomagn. Geoelectr.,* **12**(3), 148–164.

Kushiro, I., 1960. γ–α transition in Fe_2O_3 with pressure, *J. Geomagn. Geoelecr.,* **11,** 148–151.

Laberty, C. & Navrotsky, A., 1998. Energetics of stable and metastable low-temperature iron oxides and oxyhydroxides, *Geochim. Cosmochim. Acta,* **62,** 2905–2913.

Lepin', L.K. & Ruplis, A.A., 1971. *Adsorbents: Synthesis, Properties and Applications* (in Russian), p. 286, Nauka, Leningrad.

Lewis, D.G. & Farmer, V.C., 1986. Infrared absorption of surface hydroxyl groups and lattice vibration in lepidocrocite (γ-FeOOH) and boehmite (γ-AlOOH), *Clay Miner.,* **21,** 93–100.

Liu, Q.S., Banerjee, S.K., Jackson, M.J., Chen, F.H., Pan, Y. & Zhu, R., 2003. An integrated study of the grain-size-dependent magnetic mineralogy of the Chinese loess/paleosol and its environmental significance, *J. Geophys. Res.,* **108**(B9), 2437, doi:10.1029/2002JB002264.

McClelland, E. & Goss, C., 1993. Self reversal of chemical magnetization on the transformation of maghemite to haematite, *Geophys. J. Int.,* **112,** 517–532.

Morales, M.P., Muñoz-Aguado, M.J., García-Palacios, J.L., Lázaro, F.J. & Serna, C.J., 1998. Coercivity enhancement in gamma-Fe_2O_3 particles dispersed at low-volume fraction, *J. Magn. Magn. Mater.,* **183,** 232–240.

Morrish, A.H. & Clark, P.E., 1974. Non-collinearity as a size effect in micropowders of γ-Fe_2O_3, in *Proceedings of the International Conference on Magnetism II, Moscow, USSR,* pp. 180–184, Nauka, Moscow.

Morrish, A.H. & Sawatsky, G.A., 1971. Mossbauer study of the gamma to alpha transformation in pure and cobalt-doped ferric oxide, in *FERRITES: Proceedings of the International Conference,* pp. 144–147, University of Tokyo Press, Tokyo.

Neél, L., 1949. Thèorie du traînage magnetique des ferromagnètiques en grains fins avec applications aux terres cuites, *Ann. Geophys.,* **5,** 99–136.

Novakova, A.A., Gendler, T.S. & Brusentsov, N.A., 1992. Study by Mössbauer spectroscopy of the properties of magnetic carriers for medicines, *Hyperfine Interact.,* **71,** 1315–1318.

Ona-Nguema, G., Abdelmoula, M., Jorand, F., Benali, O., Géhin, A., Block, J.-C. & Génin, J.-M.R., 2002. Microbial reduction of lepidocrocite γ-FeOOH by *Shewanella putrefaciens*; the formation of green rust, *Hyperfine Interact.,* **139,** 231–237.

Özdemir, Ö., 1990. High-temperature hysteresis and thermoremanence of single-domain maghemite, *Phys. Earth planet. Inter.,* **65,** 125–136.

Özdemir, Ö. & Banerjee, S.K., 1984. High temperature stability of maghemite, *Geophys. Res. Lett.,* **11,** 161–164.

Özdemir, Ö. & Dunlop, D.J., 1988. Crystallization remanent magnetization during the transformation of maghemite to hematite, *J. geophys. Res.,* **93,** 6530–6544.

Özdemir, Ö. & Dunlop, D.J., 1989. Chemico-viscous remanent magnetization in the Fe_3O_4–γ-Fe_2O_3 system, *Science,* **243,** 1043–1047.

Özdemir, Ö. & Dunlop, D.J., 1993. Chemical remanent magnetization during γ-FeOOH phase transformation, *J. geophys. Res.,* **98**(B3), 4191–4198.

Ozima, M. & Ozima, M., 1972. Activation energy of unmixing of titanomaghemite, *Phys. Earth planet. Inter.,* **5,** 87–89.

Roberts, A.P., Cui, Y. & Verosub, K.L., 1995. Wasp-waisted hysteresis loops: Mineral magnetic characteristics and discrimination of components in mixed magnetic systems, *J. geophys. Res.,* **100,** 17 909–17 924.

Rybak, R.S., 1971. About the maghemite diagnostic ability by thermomagnetic method (in Russian), *Izv. Akad. Nauk USSR, Fiz. Zem.,* **4,** 98–101.

Sakash, G.S. & Solntseva, L.S., 1971. Mechanism of thermal decomposition of synthesized γ-Fe-oxyhydroxide (in Russian), *J. Appl. Spectrosc.,* **16,** 741.

Schwertmann, U., 1988. Some properties of soil and synthetic iron oxides, in *Iron in Soils and Clay Minerals,* pp. 267–308, eds Stucki, J.W. Goodman, B.A. & Shwertmann, U., Reidel, Norwell, MA.

Schwertmann, U. & Cornell, R.M., 1991. *Iron Oxides in the Laboratory,* VCH, Weinheim.

Shcherbakov, V.P. & Shcherbakova, V.V., 2001. On suitability of the Thellier method of paleointensity determinations to pseudosingledomain and multidomain grains, *Geophys. J. Int.,* **146,** 20–30.

Shcherbakov, V.P., McClelland, E. & Shcherbakova, V.V., 1993. A model of multidomain thermoremanent magnetization incorporating temperature-variable domain-structure, *J. geophys. Res.,* **98,** 6201–6216.

Stokking, L. & Tauxe, L., 1987. Acquisition of chemical remanent magnetization by synthetic iron oxide, *Nature,* **327,** 610–612.

Stoner, E.C. & Wolfarth, E.P., 1948. A mechanism of magnetic hysteresis in heterogeneous alloys, *Phil. Trans. R. Soc. Lond.,* A, **240,** 599–642.

Subrt, J., Hanousek, F., Zapletal, V., Lipka, J. & Hucl, M., 1981. Dehydration of synthetic lepidocrocite (γ-FeOOH), *J. Therm. Anal.,* **20,** 61–69.

Takada, T., Kiyama, M. & Shimizu, S., 1964. Morphological and crystallographical studies on the oriented transformation in γ-FeOOH and its decomposed oxides, *Bull, Inst. Chem. Res. Kyoto Univ.,* **42,** 505–510.

Takei, N. & Chiba, S., 1966. Vacancy ordering in epitaxially-grown single crystals of γ-Fe_2O_3, *J. Phys. Soc. Japan,* **21,** 1255–1263.

Tauxe, L., Mullender, T.A.T. & Pick, T., 1996. Potbellies, wasp-waists and superparamagnetism in magnetic hysteresis, *J. geophys. Res.,* **101,** 571–583.

Van Oorschot, I.H.M. & Dekkers, M.J., 1999. Dissolution behaviour of fine-grained magnetite and maghemite in the citrate-bicarbonate-dithionite extraction method, *Earth planet. Sci. Lett.,* **167,** 283–295.

Van Oosterhout, G.W. & Rooijmans, C.J.M., 1958. A new superstructure in gamma-ferric oxide, *Nature,* **181,** 44.

Von Keller, P., 1976. Thermogravimetrische Untersuchungen von Goethit und Lepidokrokit von deren Synthesprodukten α-FeOOH und γ-FeOOH, *Neues Jahrb. Miner. Monat.,* **3,** 115–127.

Waychunas, G.A., 1991. Crystal chemistry of oxides and oxyhydroxides. in *Oxide Minerals,* Reviews in Mineralogy 25, pp. 11–68, ed. Lindsley, D.H., Mineralogical Society of America, Washington DC.

Worm, H.-U. & Jackson, M., 1999. The superparamagnetism of Yucca Mountain Tuff, *J. geophys. Res.,* **104,** 25 415–25 425.